Chapter 3

Thermodynamic Modelling and Analysis of Different R-744 Cycles

This chapter presents a systematic investigation of the ejector expansion R-744 refrigeration systems based on the First and Second law of thermodynamics for different operating parameters. The effect of various operating parameters such as gas cooler exit pressure, gas cooler exit temperature, evaporator temperature etc. on the COP, pressure recovery, entrainment ratio and second law efficiency are investigated. Further, new configurations for single and multi-ejector R-744 systems are investigated for maximizing the COP of overall refrigeration system. The effect of suction nozzle pressure drop and subcooling on system performance are also investigated. An year-round operation strategy along with a control system is also investigated for thirty cities spread over five climatic zones across India. A comparison is finally presented between R-744 and R-744A based refrigeration systems.

3.1 Modeling of the Basic Ejector Expansion R744 System

In this section, we present the thermodynamic modeling of a basic ejector expansion, transcritical R744 refrigeration cycle. We present the energy and exergy balance relations for the various components in the basic cycle. In the following, we refer to the simple ejector expansion transcritical refrigeration cycle by EETRC.

3.1.1 Thermodynamic modeling and simulation strategy for the basic ejector expansion R-744 system

A simple ejector expansion transcritical refrigeration cycle (EETRC) is conceived as having a compressor, a gas cooler, a two phase ejector, a liquid vapor separator, a control valve and an 3.1) shows the schematic and $P-h$ chart of ejector expansion transcritical refrigeration cycle. The modelling of basic ejector expansion refrigeration cycle is based on one unit of two phase refrigerant mass at the outlet of the ejector. The entrainment ratio (U) is defined as the ratio of suction mass flow rate to the motive mass flow rate. For unit mass of refrigerant mixture at ejector outlet, the motive mass flow rate is $1/(1+U)$ kg and suction mass flow rate is $U/(1+U)$ kg.

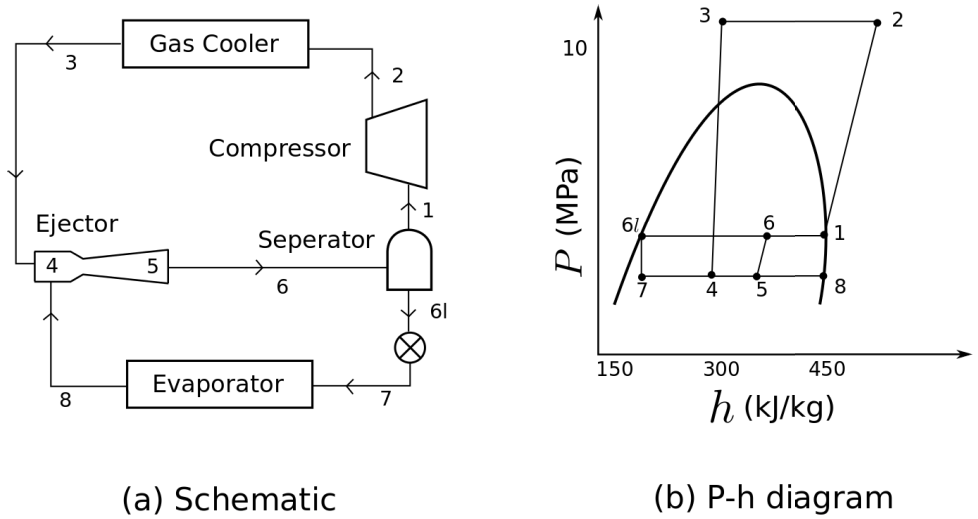

FIGURE 3.1: Schematic of ejector expansion transcritical refrigeration cycle and $P-h$ chart.

Assumptions:

- The model is developed for steady-state condition.
- At the inlet and outlet of the ejector, the kinetic energy of the refrigerant is neglected.
- The 'approach temperature' which is defined as the difference between gas cooler outlet temperature and ambient temperature is taken as 2°C.
- Saturated vapor is obtained at the evaporator exit.
- Constant pressure mixing is assumed in the mixing section. The pressure is assumed to be equal to evaporator pressure.

3.1.2 Energy balance equations

The various energy balance relations used while investigating the ejector expansion refrigeration cycle are the following:

For compressor, the power consumption per unit mass of the mixture is given by

$$W_c = \frac{h_2 - h_1}{1 + U}. \tag{3.1}$$

111]) for the compressor is

$$\eta_C = 1.003 - 0.121(\frac{P_{gc}}{P_{suc}}). \tag{3.2}$$

For the gas cooler, the heat transfer rate per unit mixed mass flow rate is given by

$$Q_{gc} = \frac{h_2 - h_3}{1 + U}. \tag{3.3}$$

The effectiveness of the gas cooler for the proposed cycle is computed from

$$E_{gc} = \frac{T_c - T_b}{T_2 - T_b}. \tag{3.4}$$

For the ejector, the motive stream enters the ejector and expands to evaporator pressure P_{evap} with a nozzle efficiency given by

$$\eta_m = \frac{h_3 - h_4}{h_3 - h_{4s}}. \tag{3.5}$$

The energy balance in the motive nozzle of the ejector is given by

$$h_3 - h_4 = \frac{V_4^2}{2}. \tag{3.6}$$

The conservation of momentum in the ejector's mixing section is given by

$$V_5 = \frac{V_4}{1 + U}. \tag{3.7}$$

The energy balance for the ejector is given by

$$h_6 = \frac{h_3}{1 + U} + \frac{h_8 U}{1 + U}. \tag{3.8}$$

The energy balance in the ejector's diffuser section is given by

$$h_6 - h_5 = \frac{V_5^2}{2}. \tag{3.9}$$

The refrigerant mixture gets pressure recovery in the diffuser section of the ejector with a given efficiency of

$$\eta_d = \frac{h_{6s} - h_5}{h_6 - h_5}. \tag{3.10}$$

The relationship between refrigerant mixture quality at ejector outlet and ejector entrainment ratio is given by

$$x_6 = \frac{1}{1+U}. \tag{3.11}$$

For the expansion valve, we have

$$h_7 = h_{6l}. \tag{3.12}$$

For the evaporator, the cooling capacity per unit of mixture mass flow rate is given by

$$Q_{evap} = \frac{(h_8 - h_7)U}{1+U}. \tag{3.13}$$

COP is used as a measure of system performance and is given by

$$COP = \frac{U}{1+U} * \frac{h_8 - h_7}{W_C}. \tag{3.14}$$

Finally, the second law efficiency for the cycle is given by

$$\eta_{second} = \frac{W_{rev}}{W_C}. \tag{3.15}$$

3.1.3 Exergy equations

The exergy destruction rate is calculated using the Gouy-Stodola theorem which says that $I = T_0 S_{gen}$. For each individual component of EETRC, the exergy destruction rate per unit mass flow rate through various components are expressed by the following relations:

- For compressor: $I_c = \frac{T_0(S_2 - S_1)}{1+U}$
- For gas cooler: $I_{gc} = \frac{T_0(S_3 - S_2)}{1+U}$
- For ejector: $I_{eje} = T_0 \left(S_6 - \frac{S_3}{1+U} - \frac{S_8 U}{1+U} \right)$
- For evaporator: $I_{evap} = T_0 \left(S_8 - S_7 + \frac{h_7 - h_8}{T_{\text{ref}}} \right) * \frac{U}{1+U}$
- For expansion valve: $I_{exp} = T_0(S_7 - S_{6l}) * \frac{U}{1+U}$

The total exergy destruction of the cycle is sum of individual component exergy destruction rate:

$$I_t = I_C + I_{gc} + I_{eje} + I_{exp} + I_{evap}. \tag{3.16}$$

The exergy balance for the cycle is given by

$$W_c = W_{rev} + I_t. \tag{3.17}$$

Based on above equations, steady stage simulation for the ejector expansion R-744 transcritical refrigeration cycles are carried out in MATLAB. The state properties are computed using NIST

3.2) shows the flow chart of the simulation for EETRC. Matlab

A

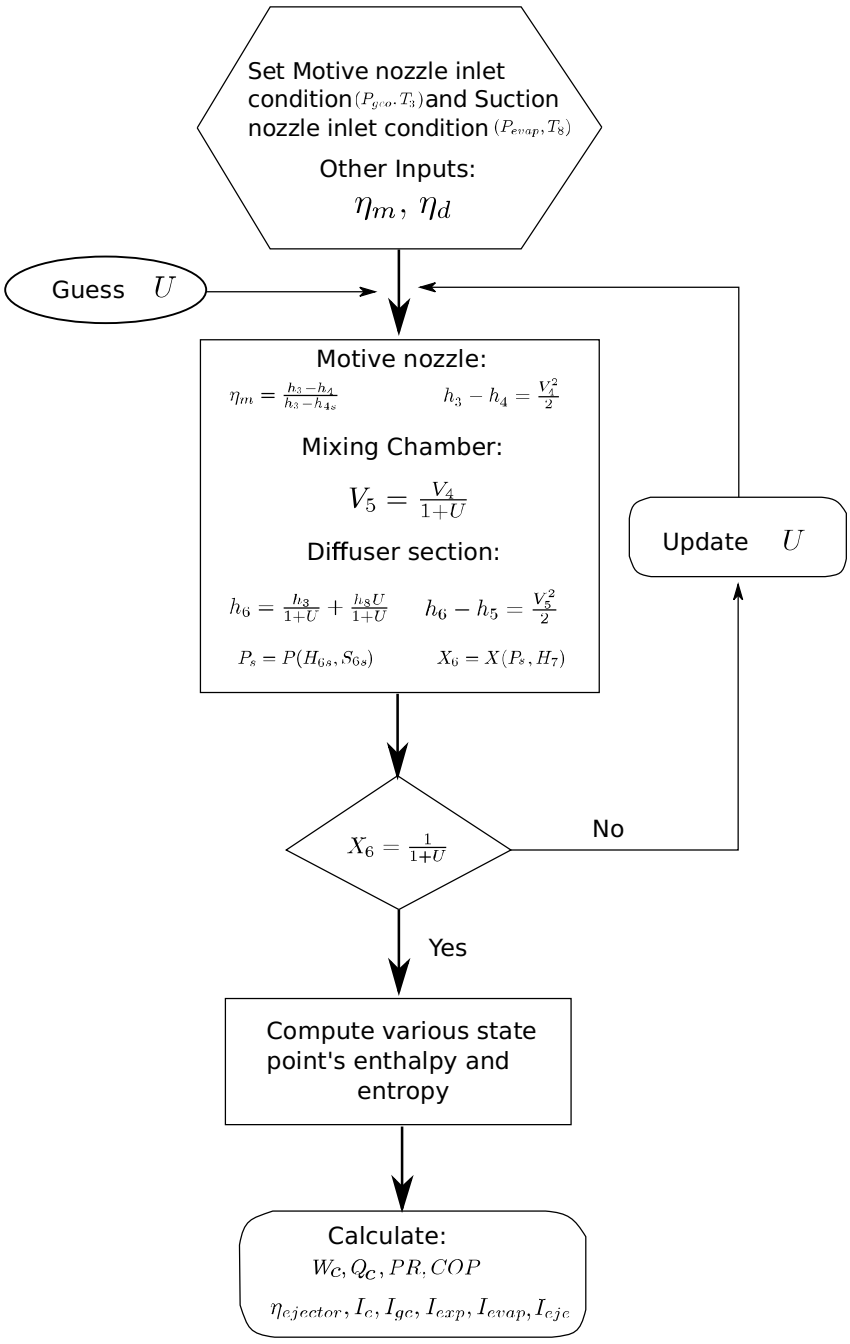

FIGURE 3.2: Flow chart of the EETRC simulation model.

3.3) shows the variation of COP and corresponding compressor work input with gas cooler outlet pressure at three different gas cooler outlet temperatures (T_{gco}) for EETRC. As T_{gco} increases, the COP decreases. This is due to the requirement of higher mass flow handling by the compressor. Further, it is observed that at higher T_{gco}, higher gas cooler operating pressure is needed for better system performance which also leads to higher compressor work input.

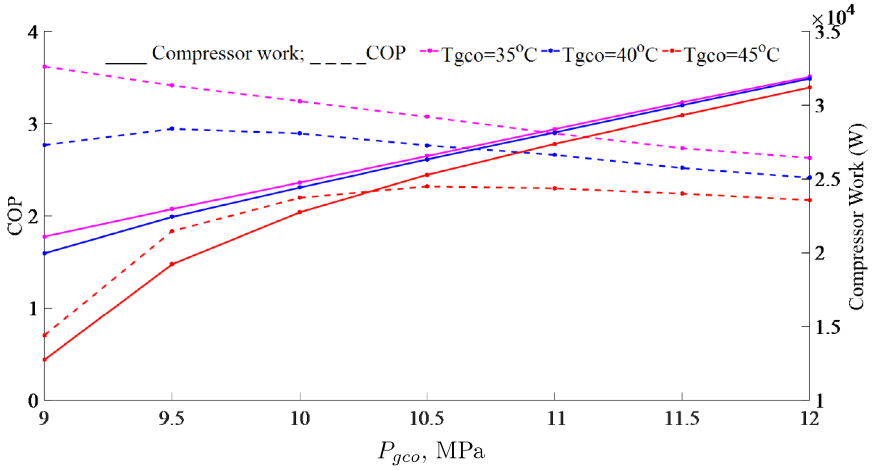

FIGURE 3.3: Variation of COP and compressor work input for the EETRC.

Exergy destruction in the various components of ejector expansion R-744 transcritical refrigeration 3.4) for fixed input condition (P_{gc} = 9.5 MPa, T_{gco} = 45°C and T_{evap}= 5°C). Exergy output of EETRC is found about 20.9%, the highest exergy destruction is found about 25.6% for expansion process in ejector. Exergy destruction associated with gas cooler and compressor are found as 24.5 % and 21.7 % respectively.

To improve COP and exergy, the basic ejector expansion transcritical R-744 refrigeration system needs modification. Exergy destruction associated with ejector can be recovered with the help of subcooling by implementing an IHX, in compressor, the same can be improved by multi-stage compression. Further, rejected heat can be used to lower the exergy destruction in gas cooler.

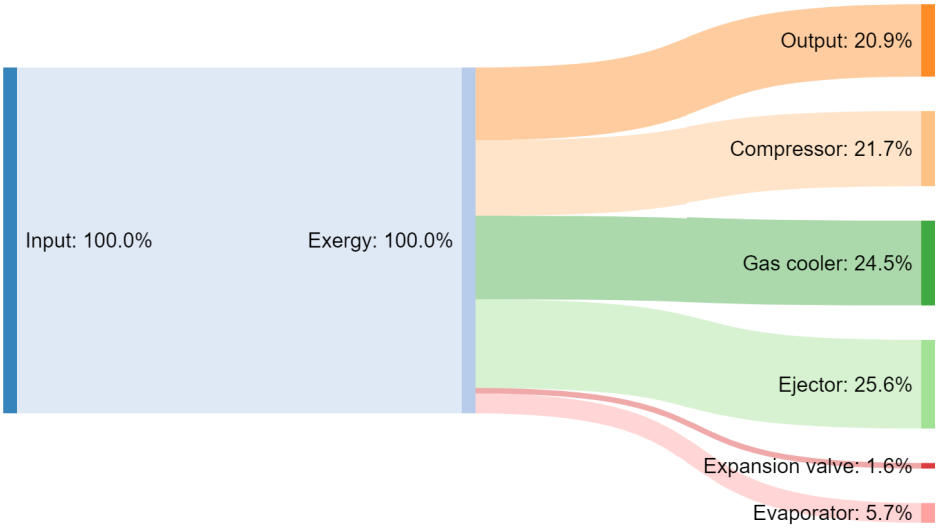

FIGURE 3.4: Exergy destruction in various components in the EETRC.

3.2 Modifications in Ejector Expansion R-744 System

Essential components like IHX, multi-stage compression, intercooler, pump, and turbine are incorporated into basic ejector cycle to arrive at modified cycles specifically for warm weather condition. A comparative study of effect of various modifications applied to basic ejector expansion R–744 transcritical refrigeration cycle is carried out to compare their applicability to high ambient (35°C-50°C). Various modified ejector expansion transcritical R-744 refrigeration systems are listed below:

- Ejector expansion R-744 transcritical system with an internal heat exchanger (EETRC+IHX).
- Multi compressor ejector expansion R-744 transcritical system with internal heat exchanger (MCEETRC+IHX).
- Multi compressor multi-intercooler ejector expansion R-744 transcritical system (MCMIEETRC).
- Multi compressor ejector expansion R-744 transcritical system in conjunction with a CO_2 power cycle (MCEETRC+CO_2 power cycle).

3.5A) shows the ejector expansion R-744 transcritical refrigeration system with IHX. The use of IHX increases the subcooling of refrigerant at gas cooler exit. This results in an increase in the refrigeration effect of the system this constitutes the EETRC+IHX system. Superheated CO_2 from IHX (state 1) enters the compressor at ejector exit pressure and undergoes compression with compressor efficiency η_C. Supercritical vapor (state 2) enters gas cooler and after constant pressure cooling, exits at temperature T_{gco} (state 3). It is further subcooled at constant pressure

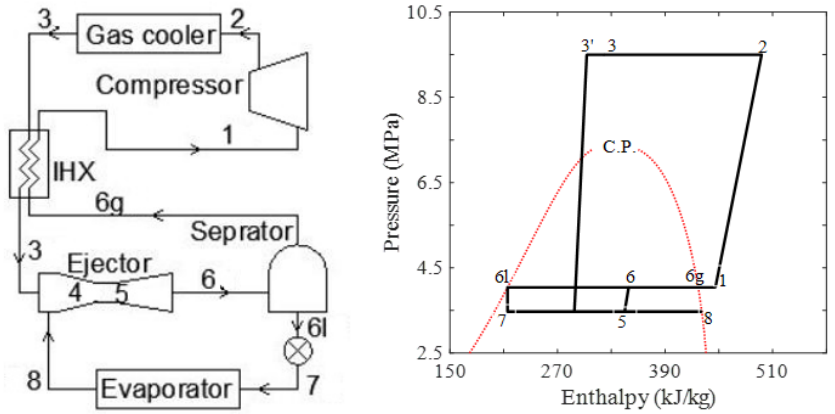

(A)

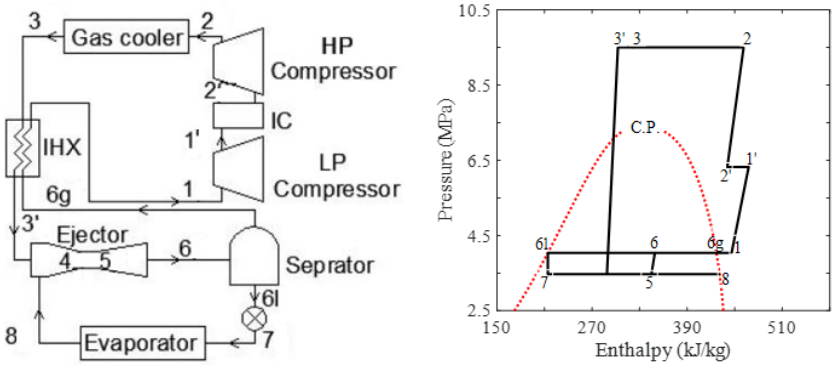

(B)

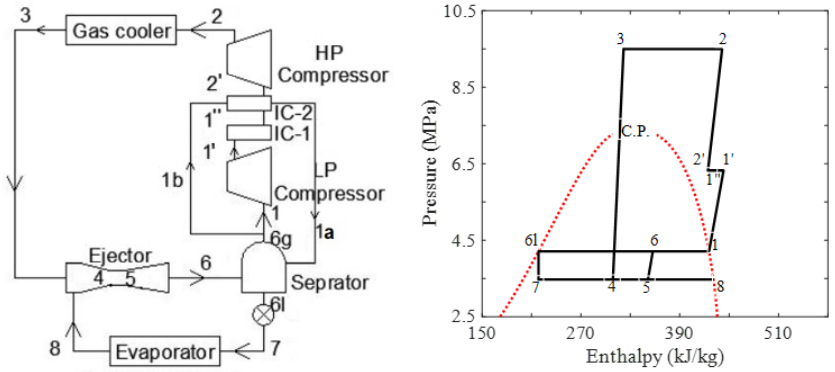

(C)

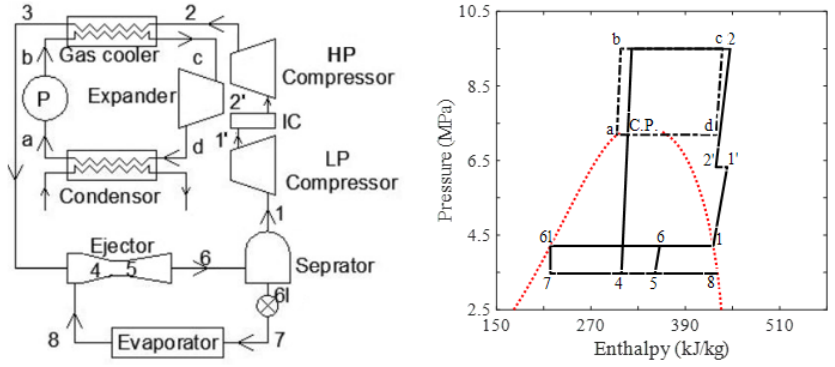

(D)

FIGURE 3.5: Schematic and pressure enthalpy chart of various ejector expansion transcritical R-744 cycles

in the IHX upto $T_{3'}$ (state 3′). After sub-cooling, the supercritical CO_2 enters the nozzle of an ejector as motive fluid and expands with nozzle efficiency (η_m). It draws secondary saturated vapor from the evaporator exit (state 8).

3.5B) shows an integration of a multi-stage compressor along with intercooler (using external fluid) in the ejector expansion R-744 transcritical refrigeration system with IHX. The addition of multi compression reduces overall compression work input due to reduced specific volume of refrigerant handled by the second compressor by the cooling of compressed vapor in the intercooler.

3.5C) shows an integration of a multi-stage compressor along with an additional second intercooler (using cycle refrigerant) after the first intercooler (using external fluid) in ejector expansion R-744 transcritical refrigeration system. The addition of the second intercooler reduces a large amount of specific volume of refrigerant handled by the second compressor by the cooling of compressed vapor in the intercooler. This results in reduction in compression work input.

3.5D) shows a combination of a multi ejector expansion R-744 transcritical refrigeration system with a supercritical CO_2 power cycle. Liquid CO_2 is pumped to gas cooler (state b) from condenser (state a). Superheated CO_2 exit from gas cooler (state c) expands in the turbine (state d). The power generated by the turbine in the CO_2 power cycle helps in the reduction of compression work of a multi compression ejector expansion R-744 transcritical refrigeration system.

Assumptions The following are assumed while doing the thermodynamic analysis of the various cycles:

- Steady state operation.
- Kinetic energies of refrigerant are neglected at the inlet and outlet of ejector.
- Approach temperature, defined as difference between gas cooler outlet temperature and ambient temperature is taken as 2°C.
- Saturated vapor is obtained at evaporator exit.
- Constant pressure mixing is assumed in the mixing section. The pressure is assumed to be equal to evaporator pressure.

The modeling of various cycles is based on one unit of two-phase refrigerant mass at the outlet 3.1. Beside above-mentioned simulation parameters, few more points are taken into consideration for analysis purpose:

TABLE 3.1: Input parameters used in the simulation.

Parameter	Value	Parameter	Value
T_0	30°C	η_m	80%
T_{evap}	-5 to 5°C	η_d	80%
T_{gc}	35 to 45°C	η_e	80%
T_{amb}	30°C	η_P	80%
T_{ref}	T_{evap} + 5°C	E_{ic}	70%
P_{gc}	9 to 12 MPa	E_{gc}	85%

- Unless stated otherwise, the refrigerant temperature at the gas cooler outlet is 40°C and the evaporating temperature is 5°C.
- The vapor is subcooled by 3°C in the internal heat exchanger before entering the motive nozzle in the internal heat exchanger cycle.
- The refrigerant flow referred as 1a in Fig 4.5(c) is superheated by 5°C at the intercooler 2 and the mass flow rate (M_{ic}) is set to 0.3 units of refrigerant mass.

3.2.1 Energy based investigations

The thermodynamic relations used in the simulation for energy are given by the following equations. For a single compressor cycle, the power consumption per unit mass of mixture is given by

$$W_C = \frac{h_2 - h_1}{1 + U}. \tag{3.18}$$

111], the adiabatic compression efficiency for the compressor is given by

$$\eta_C = 1.003 - 0.121\frac{P_{gc}}{P_{suc}}. \tag{3.19}$$

For multi compressor cycle, the power consumption of the first stage and second stage compression are given by

$$\begin{aligned} W_{C1} &= \tfrac{h_{1'} - h_1}{1+U}, \\ W_{C2} &= \tfrac{h_2 - h_{2'}}{1+U}. \end{aligned} \tag{3.20}$$

111], the adiabatic compression efficiency for first and second stage compression are given by

$$\begin{aligned} \eta_{C1} &= 1.003 - 0.121\tfrac{P_{int}}{P_{suc}}, \\ \eta_{C2} &= 1.003 - 0.121\tfrac{P_{gc}}{P_{int}}. \end{aligned} \tag{3.21}$$

The optimum intercooler pressure is obtained using

$$P_{int} = \sqrt{P_{gc} P_{suc}}. \tag{3.22}$$

The effectiveness of the intercooler is obtained using

$$E_{ic} = \frac{T_{1'} - T_{2'}}{T_{1'} - T_{amb}}. \tag{3.23}$$

The gas cooler heat transfer rate per unit mixed mass flow rate is given by

$$Q_{gc} = \frac{h_2 - h_3}{1 + U}. \tag{3.24}$$

The effectiveness of the gas cooler for the CO_2 power cycle is computed from

$$E_{gc} = \frac{T_c - T_b}{T_2 - T_b}. \tag{3.25}$$

For internal heat exchanger, the heat transfer rate is computed from

$$\begin{aligned} Q_{ihx} &= \frac{h_3 - h_{3'}}{1 + U} \text{ or} \\ Q_{ihx} &= \frac{h_1 - h_{5g}}{1 + U}. \end{aligned} \tag{3.26}$$

The effectiveness of the internal heat exchanger is computed from

$$E_{ihx} = \frac{T_1 - T_{6g}}{T_3 - T_{6g}}. \tag{3.27}$$

The motive stream enters the ejector and expands to evaporator pressure P_{evap} with a nozzle efficiency that is computed with relation

$$\eta_m = \frac{h_3 - h_4}{h_3 - h_{4s}}. \tag{3.28}$$

The energy balance in the motive nozzle is

$$h_3 - h_4 = \frac{V_4^2}{2}. \tag{3.29}$$

The suction stream entrains and expands to mixing pressure with a nozzle efficiency that is computed with relation (if SNPD is considered)

$$\eta_{suc} = \frac{h_8 - h_{8'}}{h_8 - h_{8s}}. \tag{3.30}$$

The energy balance in the suction nozzle is

$$h_8 - h_{8'} = \frac{V_{8'}^2}{2}. \tag{3.31}$$

The conservation of momentum in the mixing section

$$V_5 = \frac{V_4}{1+U}. \tag{3.32}$$

The energy balance for the ejector is

$$h_6 = \frac{h_3}{1+U} + \frac{h_8 U}{1+U}. \tag{3.33}$$

The energy balance in the diffuser section

$$h_6 - h_5 = \frac{V_5^2}{2}. \tag{3.34}$$

The refrigerant mixture gets pressure recovery in the diffuser section of the ejector with a given efficiency of

$$\eta_d = \frac{h_{6s} - h_5}{h_6 - h_5}. \tag{3.35}$$

The relationship between refrigerant mixture quality at ejector outlet and ejector entrainment ratio is

$$x_6 = \frac{1}{1+U}. \tag{3.36}$$

For the expansion valve, we have

$$h_7 = h_{6l}. \tag{3.37}$$

For evaporator, the cooling capacity per unit mixture mass flow rate is given by

$$Q_{evap} = \frac{U(h_8 - h_7)}{1+U}. \tag{3.38}$$

The system performance is evaluated by COP which for the single-stage and the multistage compressor is given respectively by

$$COP = \frac{U}{1+U} * \frac{h_8 - h_7}{W_C} \text{ and} \tag{3.39}$$

$$COP = \frac{U}{1+U} * \frac{h_8 - h_7}{W_{C1} + W_{C2}}. \tag{3.40}$$

The ejector efficiency is given by

$$\eta_{eje} = \frac{W_{rec}}{W_{rec,max}}. \tag{3.41}$$

The pump work and pump efficiency are given by

$$W_P = (h_b - h_a)M_a \text{ and } \eta_P = \frac{\nu_a(P_b - P_a)}{h_b - h_a}. \tag{3.42}$$

Similarly, the turbine work and turbine efficiency are given by

$$W_{tur} = (h_c - h_d)M_a \text{ and } \eta_{tur} = \frac{h_c - h_d}{h_c - h_{ds}}. \tag{3.43}$$

The heat transfer in the condenser is given by

$$Q_{cond} = (h_d - h_a)M_a. \tag{3.44}$$

3.2.2 Impact on COP

The coefficient of performance is considered as one of the most important system performance 3.6) shows the variation of COP with gas cooler outlet pressure at three different gas cooler outlet temperatures (T_{gco}) for the five cycle configurations.

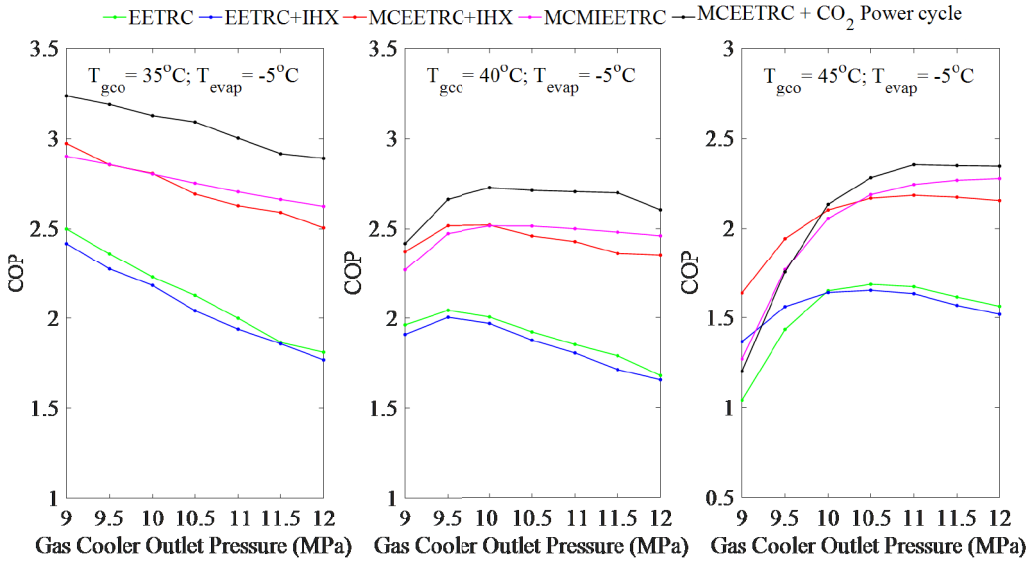

FIGURE 3.6: COP variation with gas cooler pressure under various gas cooler exit temperature.

As T_{gco} increases, the COP decreases for all cycle configurations. This is due to the enhancement of vapor quality at the ejector outlet leading to the requirement of higher mass flow handling by the compressor. The MCEETRC with supercritical CO_2 power cycle is found to have higher COP value almost for the full range of gas cooler outlet pressure. A higher $T_{gco} = 45°C$ and lower gas cooler operating pressure below 10 MPa, MCEETRC+IHX shows higher COP. This implies that subcooling is more effective in warm weather conditions at lower gas cooler operating

pressure. Further, it is also observed that at higher T_{gco}, higher gas cooler operating pressure is needed for better system performance. At higher gas cooler operating pressure, MCMIEETRC shows higher COP than MCEETRC+IHX. This can be ascribed to higher operating pressure, intercooling keeps the compression process nearer to saturation curve. The effect of the same shows overall improvement in COP than subcooling.

3.7) presents the variation of COP with gas cooler outlet pressure at three different evaporator temperatures keeping T_{gco} constant at 40°C. It is observed that as T_{evap} increases, the COP also increases. It is because, at higher evaporator temperature (and pressure), lesser refrigeration effect and compressor work is needed. There is a decrement in both refrigeration effect and compressor work with increment in T_{evap}, with increase in pressure, the same is more prominent. The MCEETRC with supercritical CO_2 power cycle shows higher COP for lower evaporating temperatures, demonstrated here for -5°C and 0°C, while that of MCMIEETRC is marginally higher at evaporating temperature 5°C. This observation can be explained as, at higher evaporating temperature, refrigerant takes lesser heat from evaporator, the same affects the heat input of CO_2 power cycle results in lesser work output.

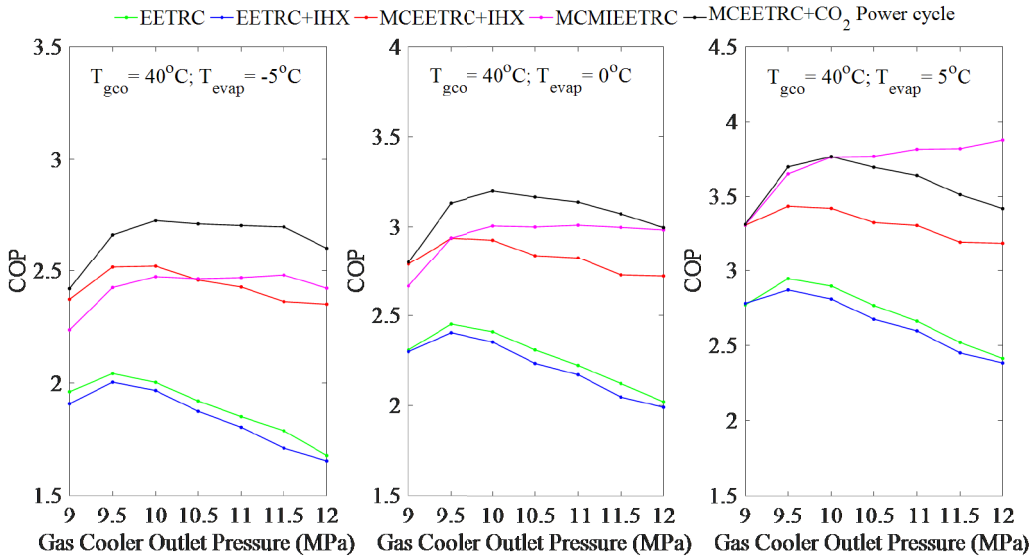

FIGURE 3.7: COP variation with gas cooler pressure under various evaporator temperature.

3.2.3 Variation in pressure recovery

The amount of pressure recovered for the various cycle configurations concerning gas cooler outlet 3.8). It is observed that the pressure recovery line for $Tgco = 45$°C is higher in all cases and there is a rapidly decreasing trend with an increase in gas cooler outlet pressure. This is since at lower T_{gco}, the energy available at the inlet of the motive nozzle is lower, which leads to lower pressure recovery. It is observed that cycle configuration having IHX shows remarkably lower pressure recovery while for other cycle configurations, pressure recovery

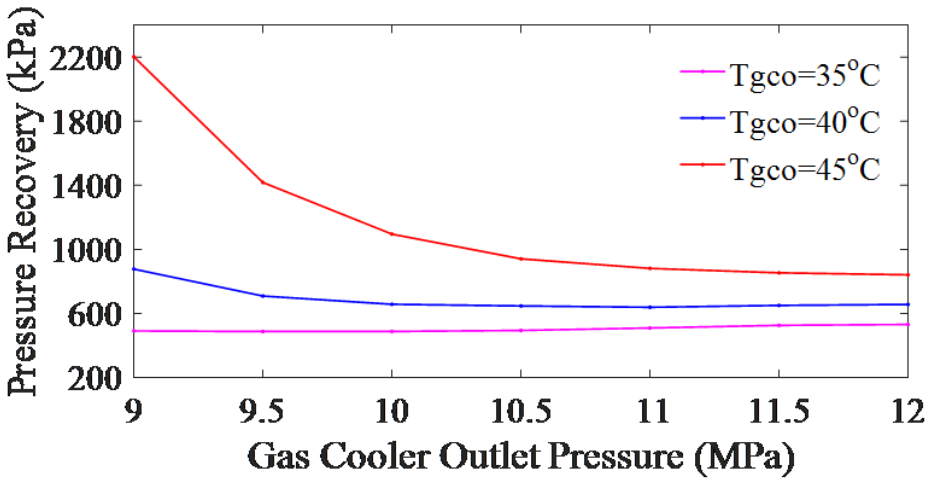

(A) EETRC, MCMIEETRC, and MCEETRC with CO_2 Power cycle

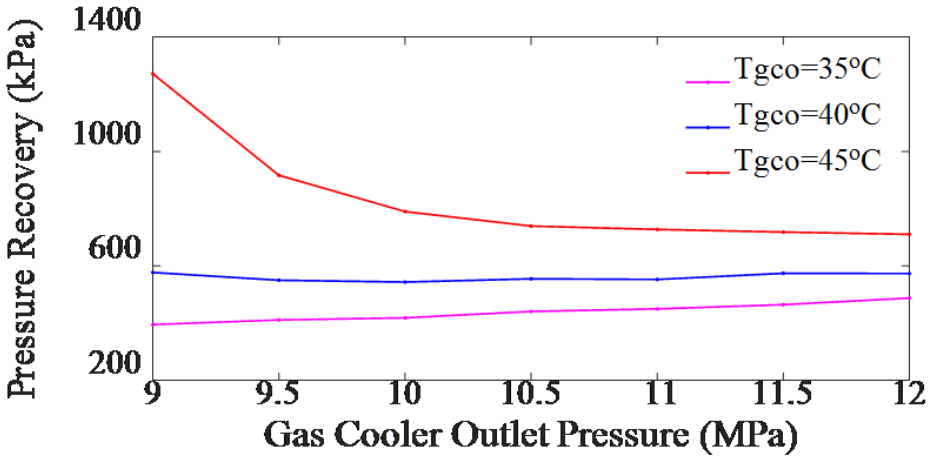

(B) EETRC + IHX and MCEETRC + IHX

FIGURE 3.8: Pressure recovery versus gas cooler pressure under various gas cooler exit temperature.

remains almost constant. Variation of pressure recovery with respect to gas cooler pressure for 3.9). It is observed that the pressure recovery is higher for a lower evaporator temperature of -5°C and the extent of pressure recovery decreases with an increase in evaporator temperature. Further, pressure recovery is found higher at lower gas cooler operating pressure for all the cycle configurations. It can be explained from the fact that a lower gas cooler outlet pressure leads to lower entrainment ratio which in turn is inversely proportional to pressure recovery. Cycle configuration employing IHX show lower overall pressure recovery while that for the MCEETRC with a supercritical-CO_2 power cycle is found similar to EETRC and MCMIEETRC.

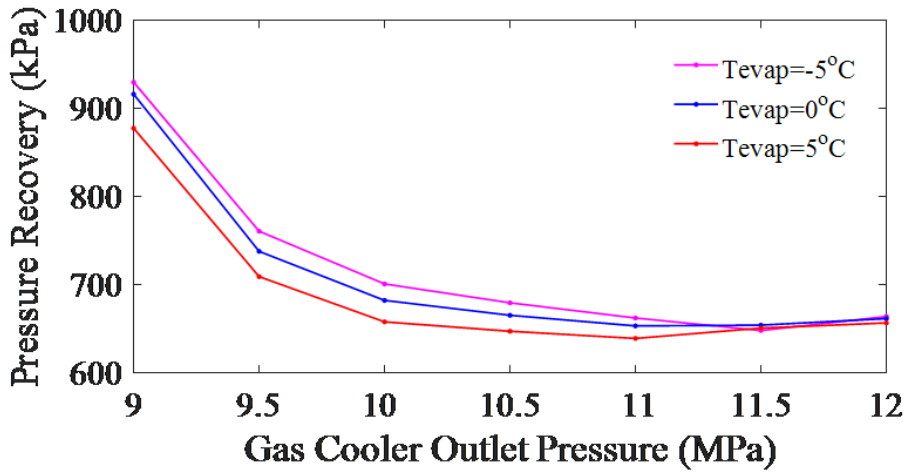

(A) EETRC, MCMIEETRC, and MCEETRC with CO_2 Power cycle

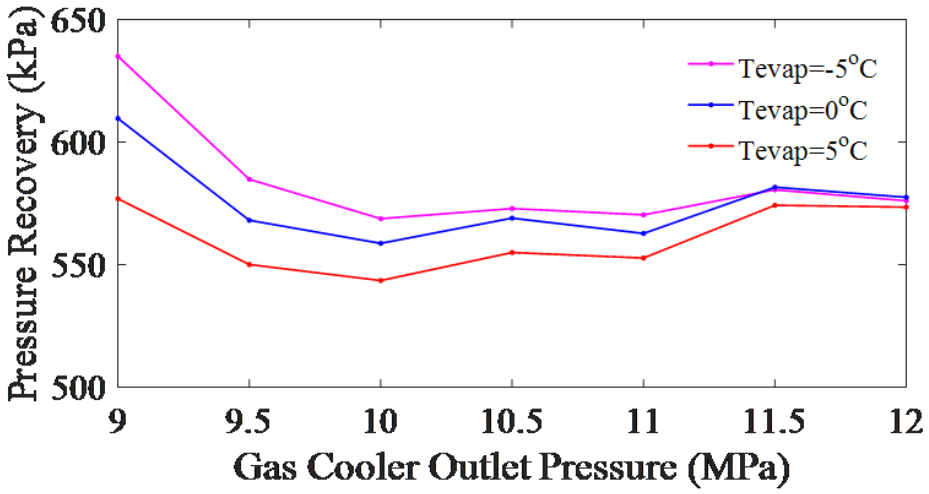

(B) EETRC + IHX and MCEETRC + IHX

FIGURE 3.9: Pressure recovery versus gas cooler pressure under various evaporator temperature.

3.2.4 Effect on entrainment ratio and vapor quality

3.10) shows the variation of entrainment ratio and vapor quality at ejector exit with changes in gas cooler outlet pressure for the three gas cooler outlet temperatures. The entrainment ratio is observed to increase rapidly and then flatten out with an increase in gas cooler outlet 3.11). It is observed that configurations without IHX have higher overall vapor quality at ejector exit and the same is most prominent for lower gas cooler outlet pressure. This implies a higher mass flow rate in compressor which leads to higher compressor work.

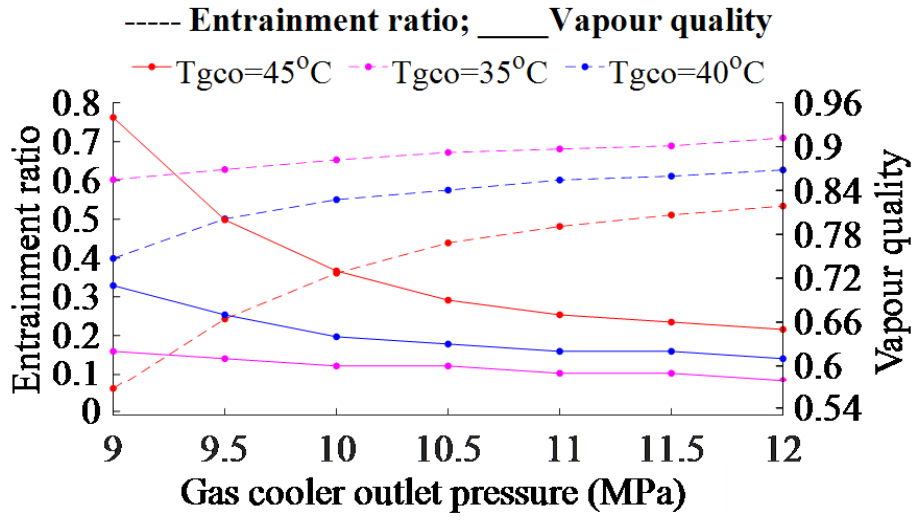

(A) EETRC, MCMIEETRC, and MCEETRC with CO_2 Power cycle

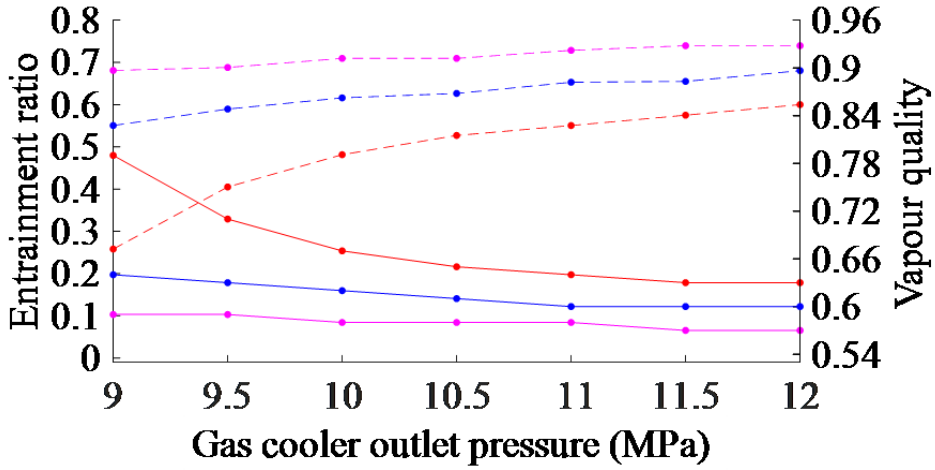

(B) EETRC + IHX and MCEETRC + IHX

FIGURE 3.10: Entrainment ratio and vapor quality versus gas cooler pressure under various gas cooler exit temperature.

3.3 Second Law Efficiency

Second law efficiency is an important criterion to judge a cycle's performance. As shown in 3.11), it is found to be maximum (26.23%) for the multi ejector expansion R-744 transcritical refrigeration system with supercritical CO_2 power cycle. For the EETRC+IHX the same is minimum at about 20.49%.

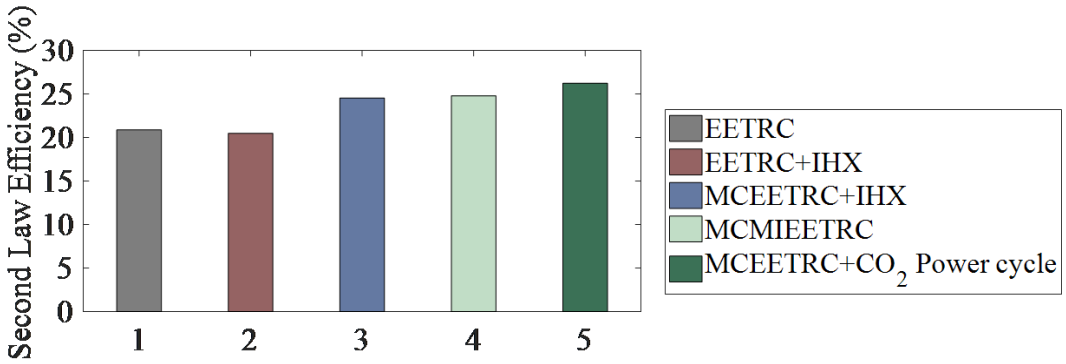

FIGURE 3.11: COP variation with gas cooler pressure under various gas cooler exit temperature.

3.3.1 Exergy investigation

An exergy analysis of each component of refrigeration systems based on the second law of thermodynamics is carried out. The exergy destruction rate is calculated by applying Gouy-Stodola theorem as

$$I = T_0 S_{gen}. \tag{3.45}$$

For each component of cycle configurations, the exergy destruction rate per unit mass flow rate through various components are expressed based on the following equations. For the compressor in the single compressor cycle, we have

$$I_C = \frac{T_0(S_2 - S_1)}{1+U}. \tag{3.46}$$

For the case of multi compressor cycle, we have

$$I_{C1} = \frac{T_0(S_{1'} - S_1)}{1+U} \text{ and } I_{C2} = \frac{T_0(S_2 - S_{s'})}{1+U}, \tag{3.47}$$

and finally,

$$I_C = I_{C1} + I_{C2}. \tag{3.48}$$

For intercoolers, we have

$$I_{ic1} = \frac{h_{1'} - h_{1''} - T_0(S_{1'} - S_{1''})}{1+U}, \tag{3.49}$$

$$I_{ic2} = \frac{h_{1''} - h_{2'} - T_0(S_{1''} - S_{2'})}{1+U}, \tag{3.50}$$

and finally,

$$I_{ic} = I_{ic1} + I_{ic2}. \tag{3.51}$$

For the gas cooler, we have

$$I_{igc} = \frac{T_0(S_3 - S_2)}{1+U}. \tag{3.52}$$

For the internal heat exchanger, we have

$$I_{ihx} = \frac{T_0(S_{3'} + S_1 - S_3 - S_{5g})}{1+U}. \tag{3.53}$$

For ejector, we have

$$I_{eje} = T_0 \left(S_5 - \frac{S_3}{1+U} - \frac{S_8 U}{1+U} \right). \tag{3.54}$$

For the evaporator, we have

$$I_{evap} = T_0 \left(S_8 - S_7 + \frac{h_7 - h_8}{T_{ref}} \right) * \frac{U}{1+U}. \tag{3.55}$$

For the expansion valve, we have

$$I_{exp} = T(S_7 - S_{6l}) * \frac{U}{1+U}. \tag{3.56}$$

For pump, we have

$$I_P = M_a T_0 (S_b - S_a). \tag{3.57}$$

For the turbine, we have

$$I_{tur} = M_a T_0 (S_d - S_c). \tag{3.58}$$

For the condenser, we have

$$I_{cond} = M_a (h_d - h_a - T_0 (S_d - S_a)). \tag{3.59}$$

The total exergy destruction of the cycle is the sum of individual component exergy destruction rate

$$I_t = I_C + I_{ic} + I_{gc} + I_{ihx} + I_{eje} + I_{exp} + I_{evap} + I_P + I_{tur} + I_{cond} \tag{3.60}$$

The exergy balance for the cycle is:

$$W_C = W_{rev} + I_t. \tag{3.61}$$

The second law efficiency for each cycle is:

$$\eta_{IInd} = \frac{W_{rev}}{W_C}. \tag{3.62}$$

Based on the above equations, exergy destruction of each component for the ejector expansion R-744 transcritical refrigeration systems are calculated.

A comparison of exergy destruction in the various ejector expansion R-744 transcritical refrigera-
3.12) for fixed input condition ($P_{gc} = 9.5$
MPa, $T_{gco} = 45$°C and $T_{evap} = 5$°C). The MCEETRC with supercritical CO_2 power cycle shows

26.22% exergy output which is highest. The MCEETRC combined with a CO_2 power cycle is successfully able to utilize the exergy loss of gas cooler, which is one of the main sources of exergy destruction for any transcritical cycle. Besides, it can be seen that the combined exergy loss of ejector and gas cooler is lowest (34.46%) for the MCEETRC with supercritical CO_2 power cycle followed by EETRC+IHX (39.98%), MCEETRC (43.89%), EETRC (50.11%)

3.13) shows the total exergy destruction and second law efficiency for the cycles. The total exergy destruction rate is maximum for EETRC+IHX, about 20.74 kJ/kg followed by EETRC (17.75 kJ/kg), MCEETRC+IHX (16.43 kJ/kg), MCMIEETRC (13.60 kJ/kg) and MCEETRC with a supercritical CO_2 power cycle (13.17 kJ/kg).

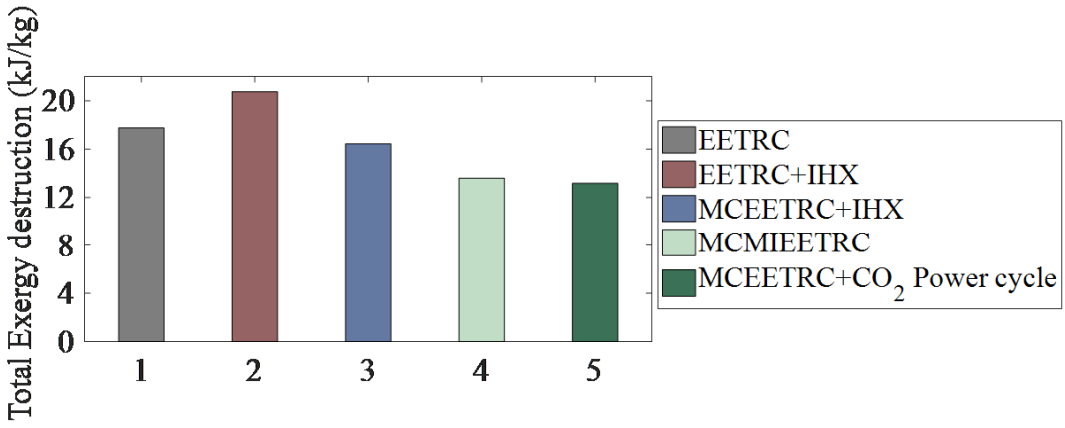

FIGURE 3.13: Total exergy destruction.

3.4 Effect of Suction Nozzle Pressure Drop

In thermodynamic modeling, mixing of the primary fluid and secondary fluid are considered in general to be mixed at evaporator pressure in an ejector expansion device. However, in practice, the mixing takes place at a pressure slightly lower than the evaporator pressure. This pressure drop is due to the refrigerant expansion while it passes through the secondary nozzle of the ejector and is called a suction nozzle pressure drop.

Suction nozzle pressure drop (SNPD) aids the flow of refrigerant from the evaporator exit to the ejector mixing chamber and is an important and sensitive parameter. The effect of SNPD on the performance of an EETRC cycle with IHX is presented for a wide range of operating conditions. Further, optimization of SNPD is carried out to maximize COP.

3.14) shows a schematic of the EETRC+IHX cycle and variation in state points of EETRC+IHX for three different SNPD values. In the EETRC+IHX system, superheated R-744 from IHX (state 1) enters the compressor at ejector exit pressure and undergoes compression with compressor efficiency η_C. Supercritical vapor (state 2) enters the gas cooler and after

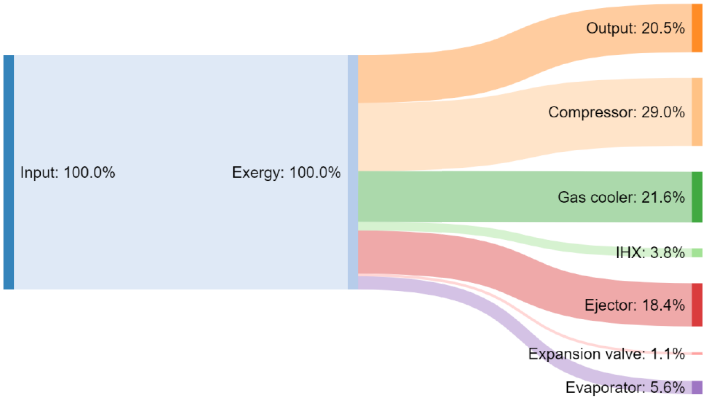

(A) EETRC+IHX

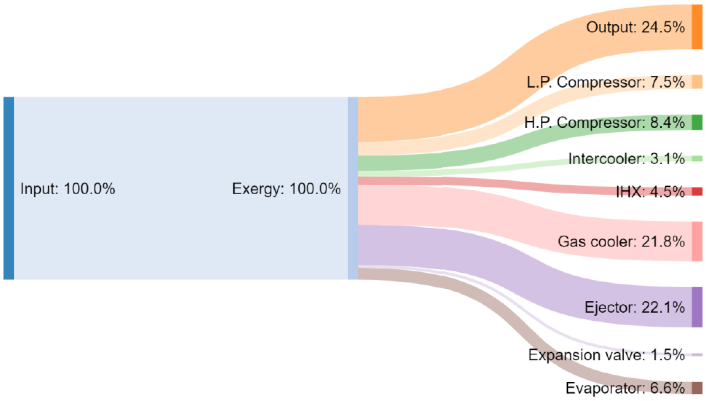

(B) MCEETRC+IHX

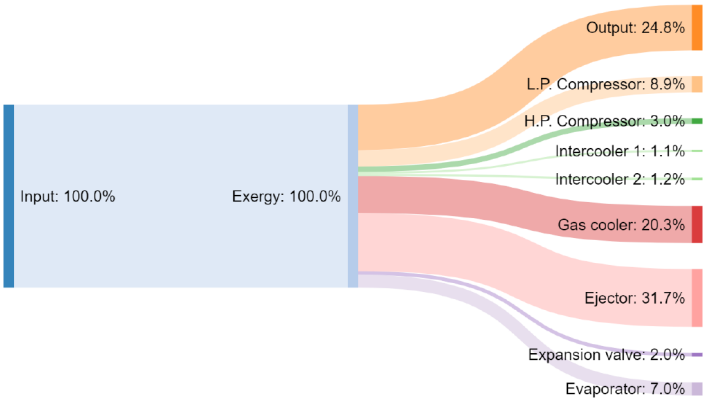

(C) MCMIEETRC

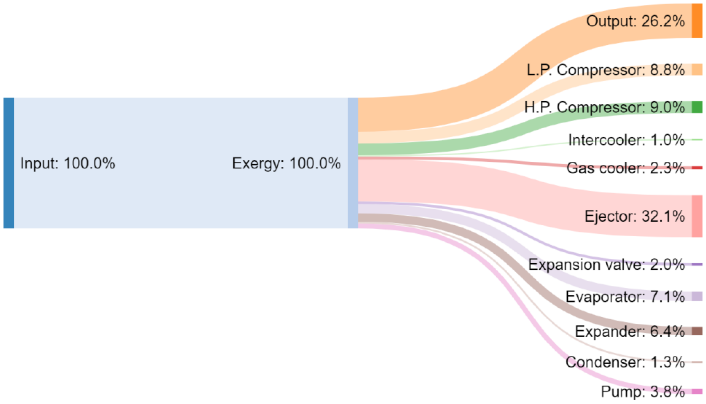

(D) MCEETRC

FIGURE 3.12: Exergy destruction for different cycles.

constant pressure cooling, exits at temperature T_{gco} (state 3). It is further subcooled at constant pressure in the IHX up to $T_{3'}$ (state 3′).

After sub-cooling, the supercritical R-744 enters in the nozzle of an ejector as motive fluid and expands with ratio $\eta_m = \frac{h_{3'}-h_4}{h_{3'}-h_{4s}}$ termed as motive nozzle efficiency (η_m). It draws secondary saturated vapor from the evaporator exit (state 8). The secondary stream gets expanded in the secondary nozzle and produces SNPD (state 8′) and gets mixed with motive stream (state 5) in the mixing chamber at constant pressure (P_{mix}).

The combined stream then flows through the diffuser section of the ejector with ratio $\eta_d = \frac{h_{6s}-h_5}{h_6-h_5}$ termed as the diffuser efficiency (η_d) and gets compressed and recovers some pressure (state 6). The ejector exit stream contains a mixed state and the same enters into a liquid-vapor separator.

From the separator, the saturated vapor is passed through an IHX (state 6g) and at the exit, superheated R-744 is obtained, then enters the compressor. The saturated liquid stream from the separator enters the control valve and expands to evaporator pressure (state 7) and produces a refrigerating effect. Thus, the two-phase ejector expansion device utilizes expansion work to gain pressure recovery and enhances the cycle performance.

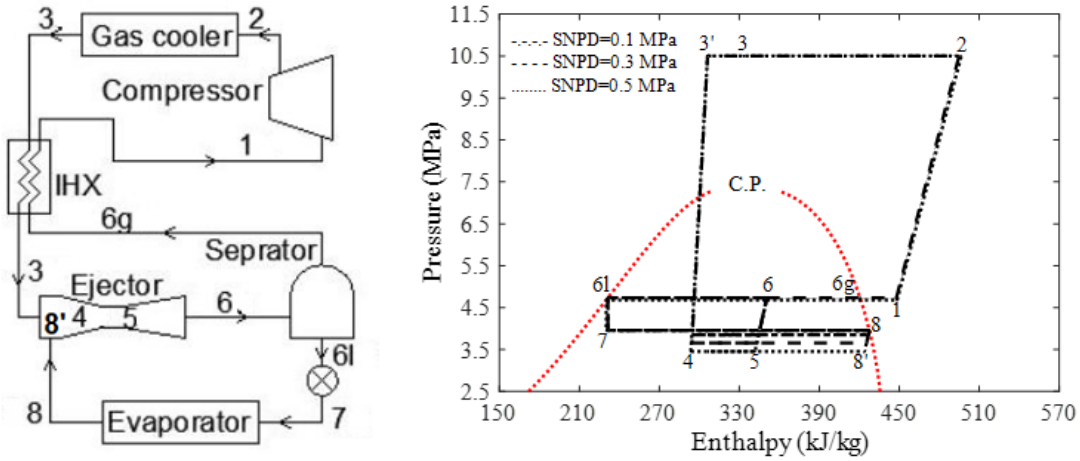

FIGURE 3.14: Schematic diagram pressure enthalpy chart for EETRC+IHX (considering SNPD)

The various assumptions for this analysis are as follows:

- The systems are simulated under steady-state conditions.
- At the inlet and outlet of an ejector, the kinetic energy of refrigerant is neglected.
- Approach temperature ($T_{gco} - T_0$) of the gas cooler is taken as 2°C.
- Unless stated otherwise, the refrigerant temperature at the gas cooler outlet (T_{gco}) is 45°C and the evaporator temperature (T_{evap}) is 5°C.

- Unless stated otherwise, the degree of sub-cooling is limited to 5°C.
- Unless stated otherwise, $\eta_m = \eta_{suc} = \eta_d$ 112 40]; Goodarzi et al. 43 42]).
- The refrigerant condition at the exit of the evaporator is a saturated vapor.
- Constant pressure mixing is assumed in the mixing section.
- Based on equations (1-28), a steady-state stage simulation for the EETRC+IHX is developed in MATLAB. State point properties are computed using NIST REFPROP version 9.0.

3.4.1 Impact on COP

3.15) shows the effect of SNPD on COP at various gas cooler outlet temperatures for a range of gas cooler pressures keeping T_{evap} constant at 5°C. As discussed earlier, it is observed that the COP decreases with an increase in T_{gco} and has a maximum value at an optimum gas cooler operating pressure.

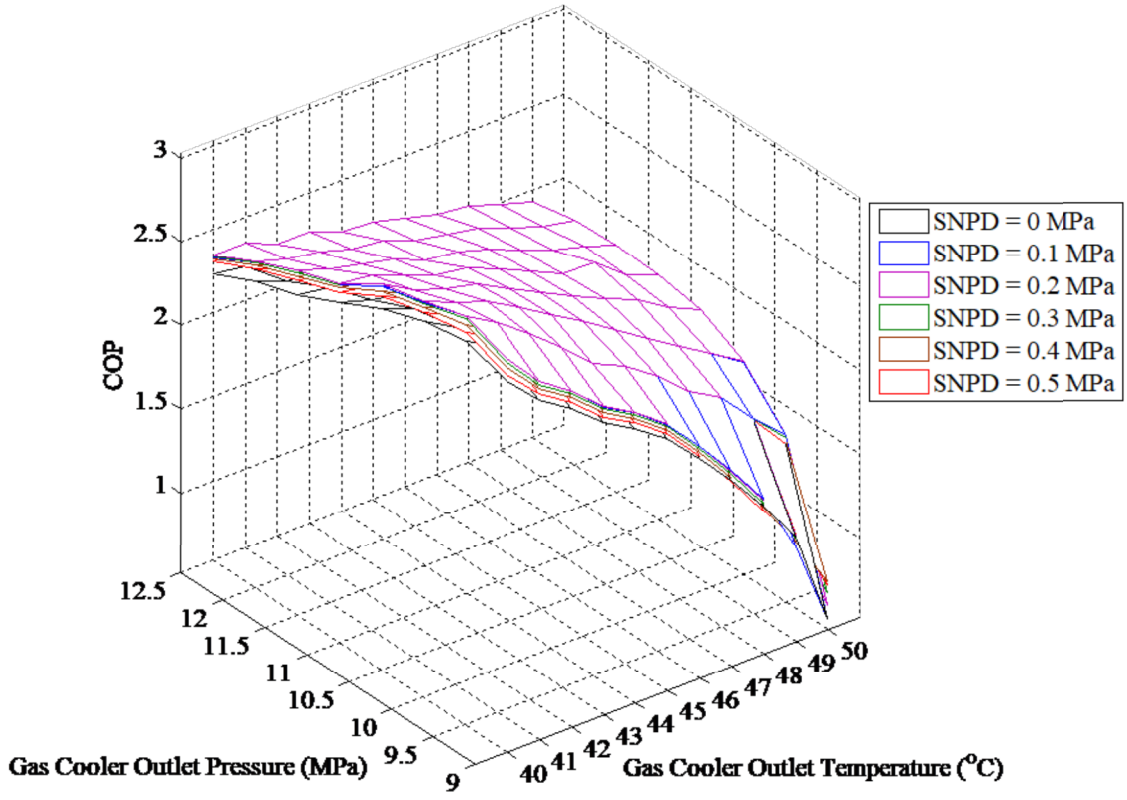

FIGURE 3.15: Variation of COP with P_{gco} under various T_{gco}.

3.15) three major conclusions are drawn:

- As gas cooler outlet pressure increases, the COP passes through a maxima for all T_{gco}.
- There is an optimum SNPD between 0.1 to 0.2 MPa for which the COP is maximum and the trend is consistent across T_{gco} variation.
- The sensitivity of COP to SNPD decreases with an increase in T_{gco}.

3.4.2 Impact on ejector efficiency

Change in ejector efficiency with gas cooler outlet pressure and gas cooler outlet temperature for 3.16). Ejector efficiency is important because it reflects the amount of pressure recovery in the ejector which in turn reduces the irreversibility 3.16) that with an increase in gas cooler outlet pressure, the ejector efficiency increases and the same is more prominent at higher T_{gco}. There is a substantial difference in ejector efficiency from a condition where SNPD is neglected to a condition where SNPD is within range 0.1 MPa to 0.5 MPa.

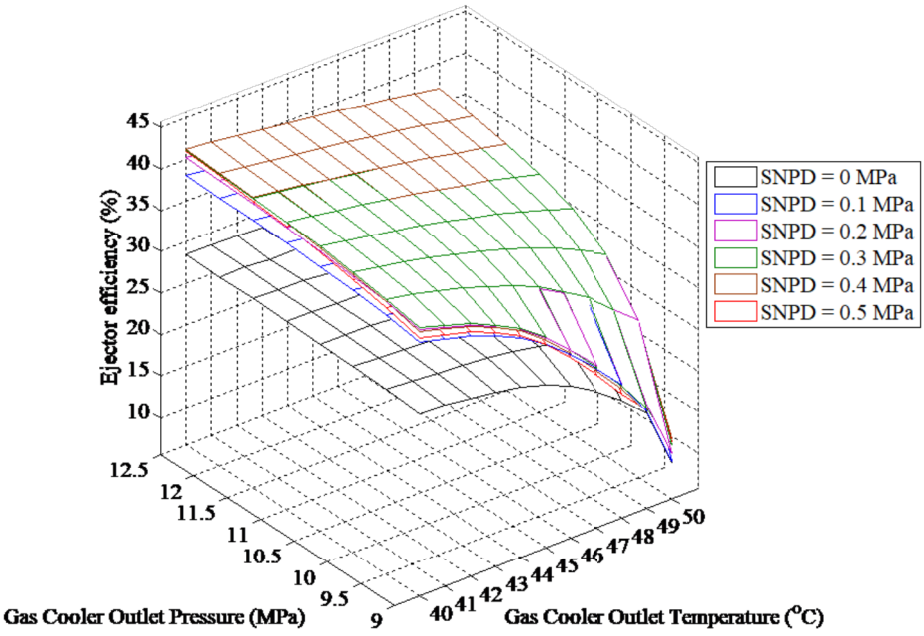

FIGURE 3.16: Ejector efficiency variation with P_{gco} under various T_{gco}

At higher gas cooler outlet pressure, the pressure energy available at the inlet of the motive nozzle is also higher which leads to higher ejector efficiency. At higher gas cooler exit temperature, the vapor quality at ejector exit is also higher at concerning gas cooler pressure, it leads lower entrainment ratio which in turn lowers the ejector efficiency at higher T_{gco}. At constant $T_{gco} = 45°C$, the effect of SNPD on ejector efficiency is further investigated for variation of T_{evap} 3.17). As expected, an increasing trend of ejector efficiency is observed with an increase in gas cooler outlet pressure across all T_{evap}.

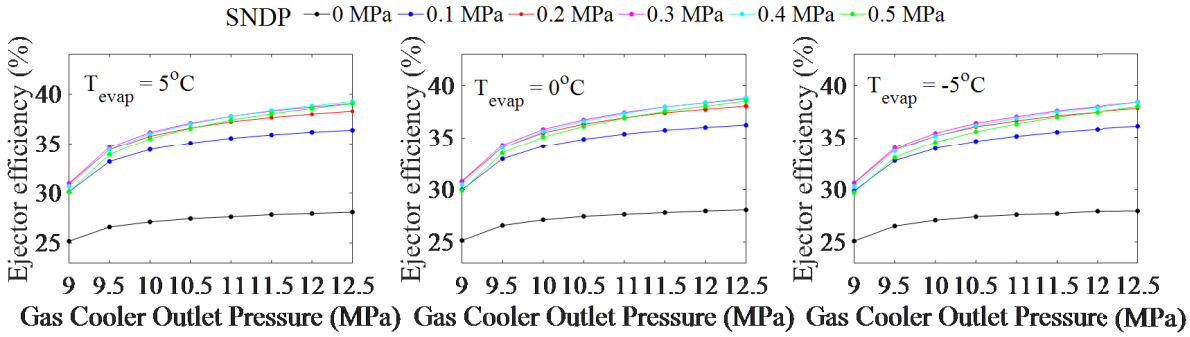

FIGURE 3.17: Ejector efficiency variation with P_{gco} under various T_{evap}.

3.4.3 Variation in pressure recovery

The amount of pressure recovery with gas cooler outlet pressure and gas cooler outlet temperature 3.18).

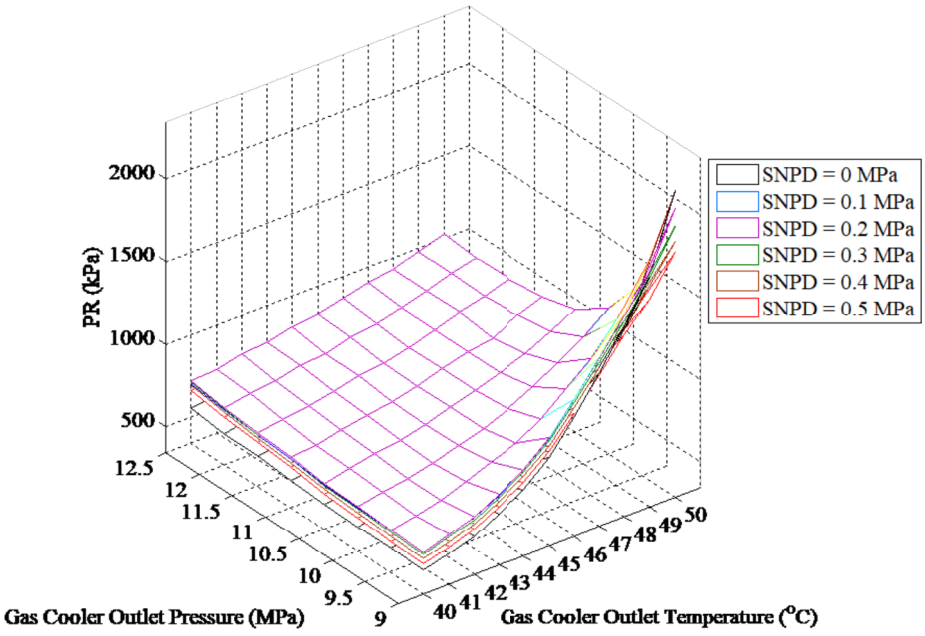

FIGURE 3.18: Pressure recovery variation with P_{gco} under various T_{gco}.

It is observed that the surfaces intersect each other, therefore, the pressure recovery trend at various T_{gco} is not similar. However, comparing across the T_{gco}, we see that at particular gas cooler outlet pressure, the pressure recovery is more sensitive to variation in SNPD at lower T_{gco}. The amount of pressure recovery increases with an increase in gas cooler outlet temperature and the same can be ascribed to the fact that more energy is available at higher gas cooler outlet temperature.

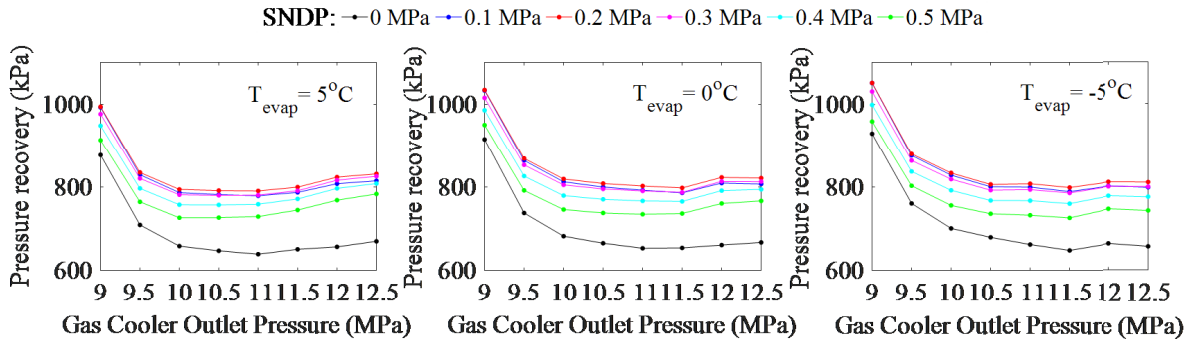

FIGURE 3.19: Pressure recovery versus P_{gco} under various T_{evap}.

Keeping T_{gco} constant at 45°C, the effect of variation of T_{evap} on pressure recovery is investigated 3.19). Beyond gas cooler pressure 9.5 MPa, it is observed that the trend at different T_{evap} is similar and there is a marginal increment in pressure recovery with the decrease in T_{evap}. This is possible because, at lower evaporator temperature, the pressure difference between motive nozzle inlet and outlet is higher. Significantly higher pressure recovery is observed at lower gas cooler pressure (below 9.5 MPa) and the reason behind the same is that at lower gas cooler pressure, the entrainment ratio is also lower which in turn leads to higher pressure recovery.

3.4.4 Effect on entrainment ratio and vapor quality

3.20) shows variation in entrainment ratio with gas cooler pressure at three different gas cooler outlet temperatures for various SNPD.

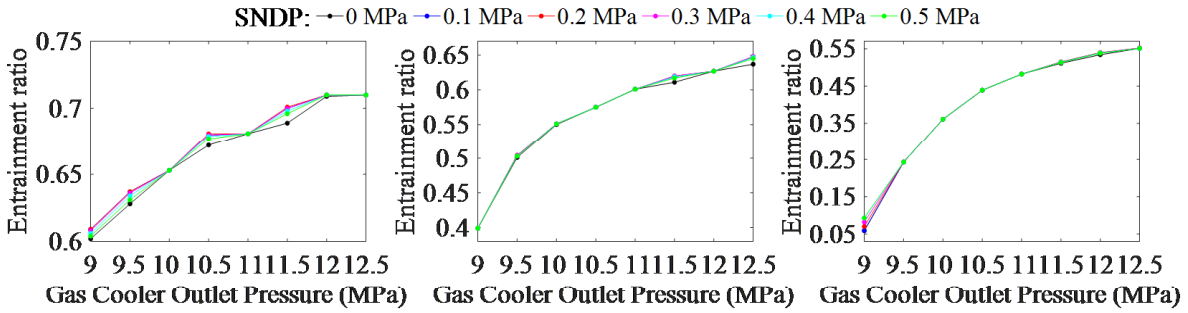

FIGURE 3.20: Entrainment ratio versus P_{gco} under various T_{gco}.

It can be observed that the entrainment ratio increases with an increase in gas cooler pressure but SNPD is observed to have very less effect on entrainment ratio. It is perceived that at higher gas cooler pressure the suction effect produced by the motive nozzle is also higher leading to increment in entrainment ratio. Further, it is observed that the entrainment ratio decreases with an increase in gas cooler temperature. It can be explained from the fact that at higher gas

cooler outlet temperature, the vapor quality produced at the ejector exit is higher which intern lowers the entrainment ratio.

3.5 Effect of Different Nozzle Velocities Inside the Ejector

The magnitude of the flow velocity of refrigerant in the mixing section of the ejector should be 47]. The flow velocities are determined by the law of conservation of momentum.

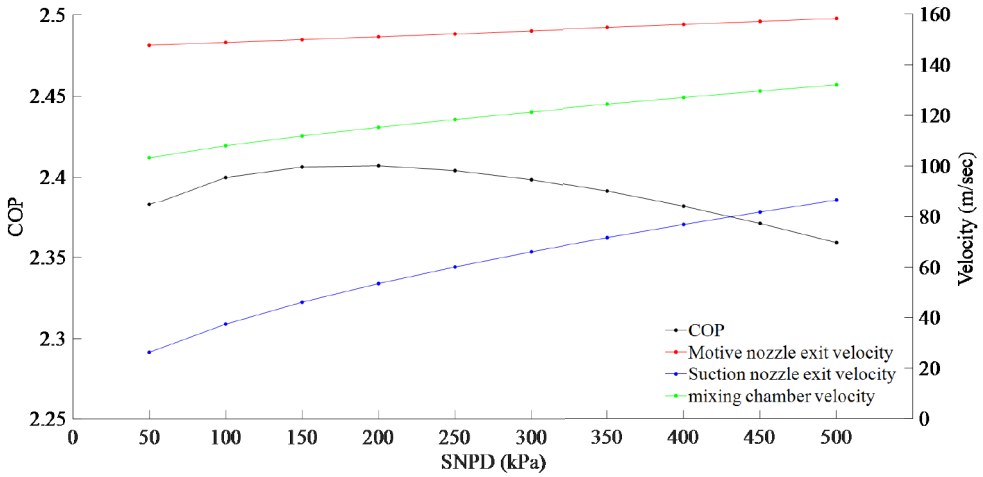

FIGURE 3.21: Influence of SNPD on COP and various ejector velocities.

3.21) shows variation of COP with SNPD, with the variation of the three important ejector velocities with SNPD in the same range. A fixed operating condition of P_{gco} = 10.5 MPa, T_{gco} = 45°C, and T_{evap} = 5°C is assumed. It is concluded that ejector velocities across the various sections increase significantly with an increase in SNPD. While there is a marginal variation of COP with SNPD which has a maxima between 0.15 to 0.20 MPa and thereafter COP steadily decreases. On a finer scale, an optimum value of SNPD of 0.18 MPa is determined later for the given condition.

3.5.1 Variation of the efficiencies of the nozzle inside the ejector

3.22) shows the variation of optimum SNPD with motive nozzle, suction nozzle, and diffuser efficiency. To calculate the optimum SNPD, the three efficiencies are varied from 10% to 90% individually in such a way that rest of the two are kept constant at 80%. The refined value of optimum SNPD found by this operation is ∼0.18 MPa, an increment of 4.95% in COP is observed at SNPD=0.18 MPa compared to SNPD=0 MPa. The exercise is repeated for P_{gco} ranging from 9.0 MPa to 12.5 MPa and T_{gco}= 40°C, 45°C, 50°C keeping T_{evap} constant at 5°C

TABLE 3.2: Optimum SNPD (MPa) for various P_{gco}, T_{gco} and nozzle efficiency.

	$T_{gco} = 40°$ C				$T_{gco} = 45°$ C				$T_{gco} = 50°$ C			
P_{gco} (MPa)	$\eta =$ 0.75	$\eta =$ 0.80	$\eta =$ 0.85	$\eta =$ 0.90	$\eta =$ 0.75	$\eta =$ 0.80	$\eta =$ 0.85	$\eta =$ 0.90	$\eta =$ 0.75	$\eta =$ 0.80	$\eta =$ 0.85	$\eta =$ 0.90
9.0	0.1	0.16	0.24	0.38	0.10	0.16	0.24	0.4	0.04	0.12	–	–
9.5	0.1	0.16	0.24	0.38	0.12	0.16	0.26	0.42	0.08	0.12	0.20	0.28
10.0	0.12	0.16	0.26	0.40	0.12	0.18	0.28	0.44	0.10	0.16	0.26	0.42
10.5	0.12	0.18	0.26	0.42	0.12	0.18	0.28	0.44	0.12	0.18	0.28	0.46
11.0	0.12	0.18	0.28	0.44	0.12	0.20	0.30	0.46	0.12	0.20	0.30	0.48
11.5	0.12	0.20	0.28	0.46	0.14	0.20	0.30	0.48	0.14	0.20	0.32	0.50
12.0	0.14	0.20	0.30	0.46	0.14	0.20	0.32	0.50	0.14	0.22	0.32	0.52
12.5	0.14	0.20	0.32	0.50	0.14	0.22	0.32	0.52	0.14	0.22	0.34	0.54

3.2 which gives a guideline to fix SNPD for a range of P_{gco}, T_{gco}

3.2 that the optimum SNPD value increases with an increase in both gas cooler pressure and various ejector nozzle efficiencies. Overall, optimum SNPD lies within the range of 0.04 MPa to 0.54 MPa for the selected operating range.

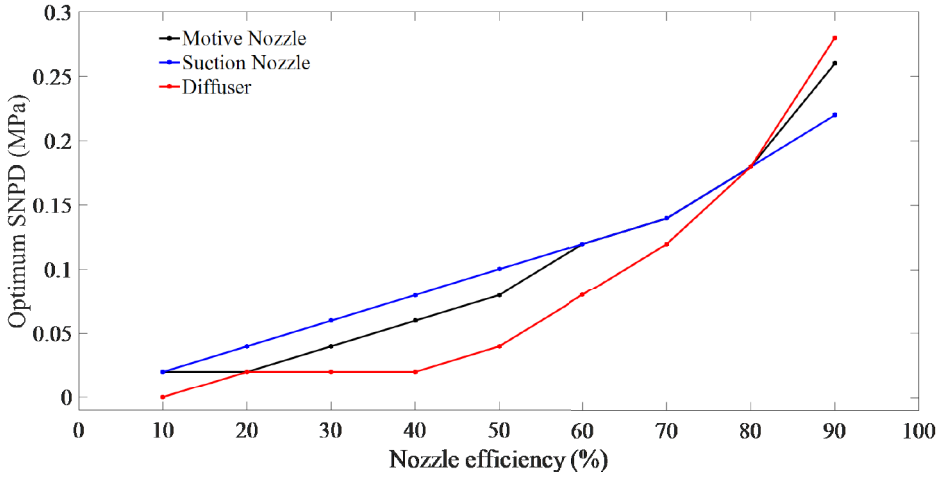

FIGURE 3.22: Optimum SNPD versus various nozzles efficiency.

3.5.2 Variation in Second law efficiency

3.23) summaries the variation of second law efficiency with respect to gas cooler pressure for EETRC+IHX with and without SNPD. It is observed that EETRC+IHX shows the higher overall second law efficiency when SNPD was taken into consideration for the entire range of operating gas cooler pressure. The flat nature of the graph implies that the EETRC+IHX can be operated for a reasonably wide range of gas cooler outlet pressure, for high second law efficiency.

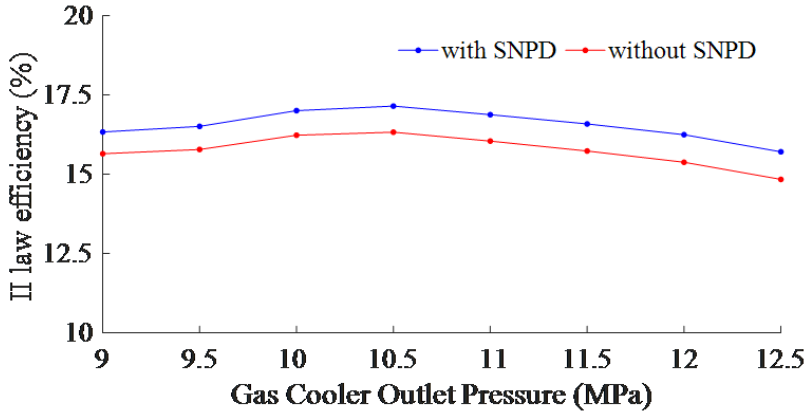

FIGURE 3.23: Second law efficiency variation with gas cooler discharge pressure.

3.6 Performance Assessment for Degree of Sub-Cooling

Sub-cooling of refrigerant in IHX at the exit of the gas cooler is known to have a positive effect on COP. The performance of the ejector depends on the motive nozzle inlet condition and sub-cooling in IHX influences the same. Further investigation is necessary to understand the effect of the degree of sub-cooling on COP of the cycle in the presence of ejector. An analysis is carried out keeping in mind the optimum SNPD for respective P_{gco} and T_{gco} to maximize COP.

3.6.1 Impact on COP

Variation of COP with respect to gas cooler outlet pressure for various degree of sub-cooling at 3.24).

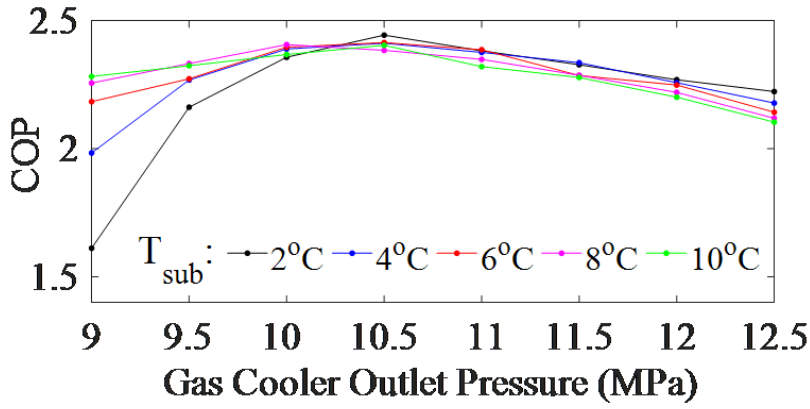

FIGURE 3.24: COP variation with gas cooler discharge pressure for sub-cooling temperatures.

It can be observed that COP passes through a maxima as gas cooler pressure increases. Further, the COP of CTRC+IHX increases with an increase in the degree of sub-cooling. This can be

explained by the fact that with an increase in sub-cooling, the refrigerating effect increases while compressor work decreases. Further, IHX helps to superheat the refrigerant at the exit of the evaporator. The degree of sub-cooling influences COP more at lower gas cooler pressure.

3.6.2 Impact on ejector efficiency

Variation of ejector efficiency with gas cooler outlet pressure at various degree of sub-cooling and 3.25). Ejector efficiency is found to have an increasing trend with an increase in gas cooler pressure. At a higher degree of sub-cooling, the ejector efficiency is higher but is less sensitive to change in gas cooler outlet pressure.

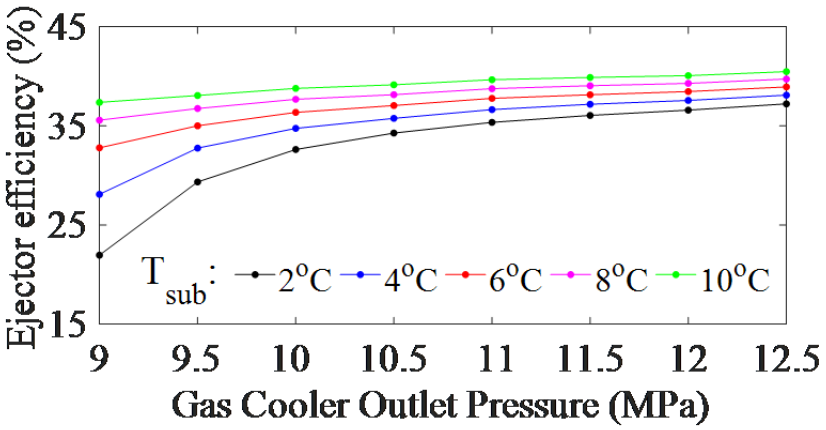

FIGURE 3.25: Ejector efficiency versus gas cooler discharge pressure for sub-cooling temperatures.

3.6.3 Variation in pressure recovery

3.26) depicts pressure recovery in the ejector versus gas cooler outlet pressure for various degree of sub-cooling at optimum SNPD.

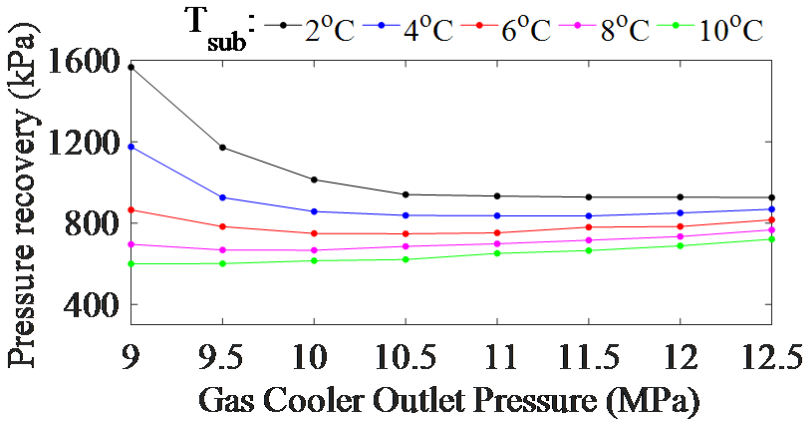

FIGURE 3.26: Pressure recovery versus P_{gco} at various sub-cooling temperatures.

TABLE 3.3: Optimum degree of sub-cooling for various P_{gco} and T_{gco} using optimum SNPD.

P_{gco} MPa	$T_{gco} = 40°C$	$T_{gco} = 45°C$	$T_{gco} = 50°C$
9.0	2°C	10°C	18°C
9.5	2°C	8°C	14°C
10.0	2°C	8°C	14°C
10.5	2°C	6°C	12°C
11.0	2°C	6°C	10°C
11.5	2°C	4°C	10°C
12.0	2°C	2°C	2°C
12.5	2°C	2°C	2°C

Pressure recovery is found to have a decreasing and converging trend with an increase in gas cooler pressure. This is because, at lower gas cooler pressure, the entrainment ratio is also low which in turn keeps the amount of pressure recovery high. Further, for a lower degree of sub-cooling, the pressure recovery is higher and the same decreases with an increase in the degree of sub-cooling.

3.6.4 Effect on entrainment ratio and vapor quality

3.27) shows entrainment ratio and vapor quality respectively with gas cooler outlet pressure at optimum SNPD. It is observed that the entrainment ratio increases whereas vapor quality decrease with an increase in gas cooler pressure as they have inverse relation as per 3.11). Further, it is observed that the entrainment ratio is higher for a higher degree of subcooling as an increase in the degree of sub-cooling leads to lower vapor quality at ejector exit. Both entrainment ratio and vapor quality are found to be more sensitive to the degree of sub-cooling at lower gas cooler outlet pressure.

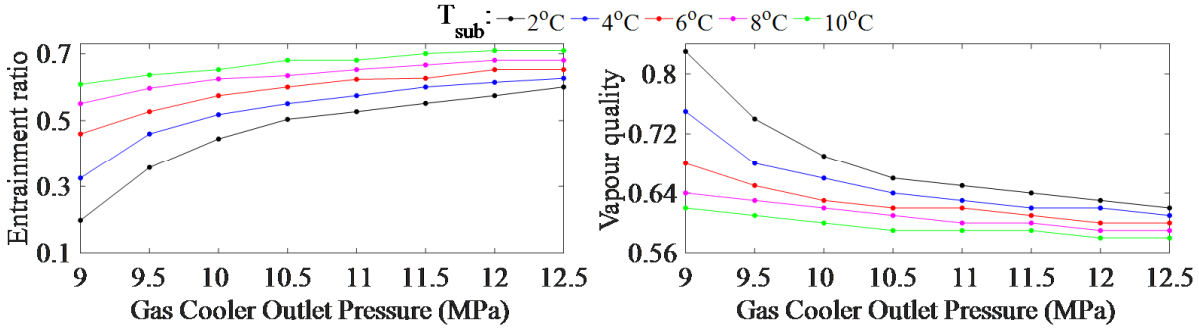

FIGURE 3.27: Entrainment ratio and vapor quality variation with gas cooler discharge pressure at various sub-cooling temperatures.

3.3 shows the optimum degree of sub-cooling for various P_{gco} and T_{gco}. It can be concluded from the tabulated data that the requirement of sub-cooling is higher with an increase in T_{gco} and a decrease in P_{gco}.

3.7 Year-Round Controlled Operation in High Ambient Conditions in India

3.7.1 Climate zones in India

There are six climate regions in India as per Koppen climate classification (www.en.wikipedia.org). These are the Arid region, Semiarid region, Tropical wet region, Tropical wet and dry region, Humid subtropical region, and Mountain/Highland climate region. Thirty highly populated cities, distributed in the five different climate zones of India are selected for this study excluding 3.28 3.29) shows the frequency of ambient temperatures recorded in these thirty cities for one year.

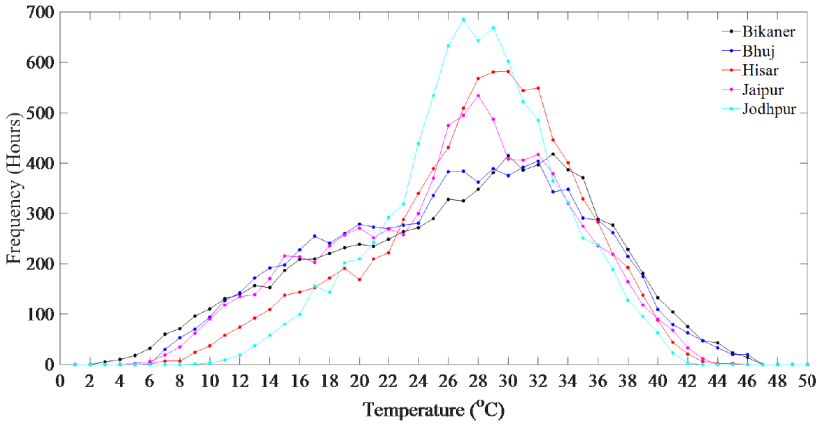

(A) Arid region

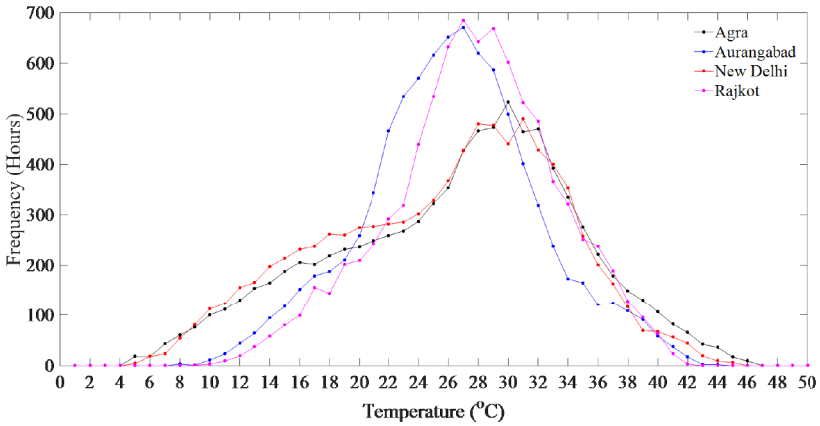

(B) Semi-arid region

FIGURE 3.28: Temperature profiles of various cities in different climate regions of India plotted 113].

The Year around hourly variation of ambient temperature data is obtained from TRANSYS-6 113] and plotted using Matlab. From the temperature distribution plot, a few important observations made are. Consistently high ambient temperature above 35°C remains for a

prolonged duration mostly in Arid and Semi-arid Regions. Within the identified cities, the duration in the number of hours for temperature above 35°C is highest for Bikaner, while the 3.4 shows year-round percentage of the time in hours under various temperature ranges for the different cities.

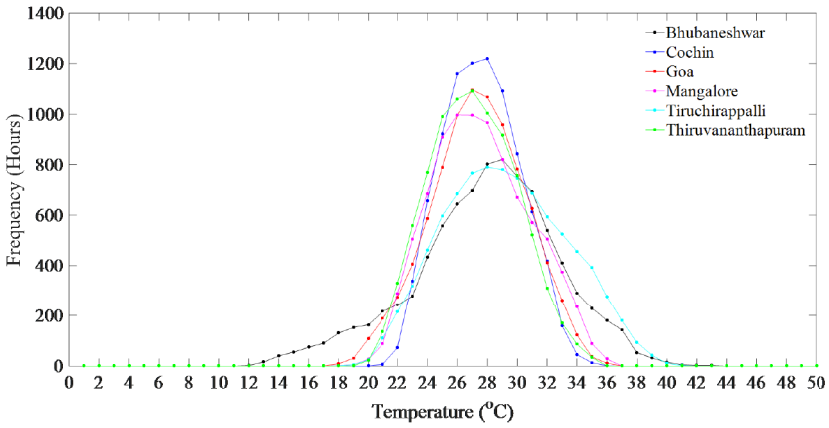

(A) Tropical wet region

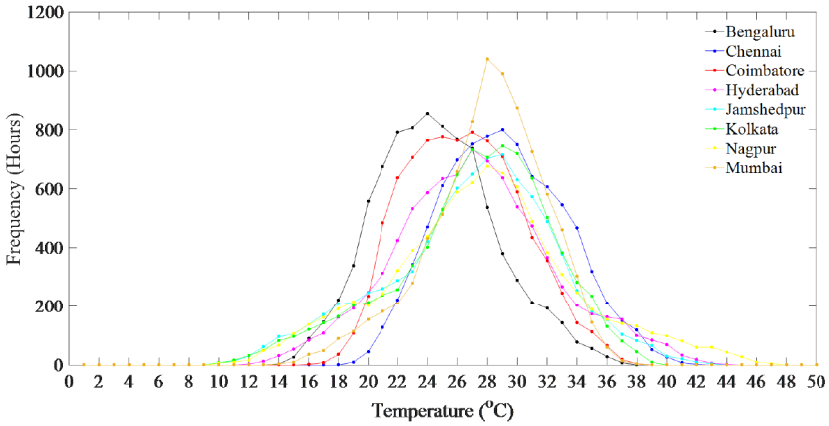

(B) Tropical wet and dry region

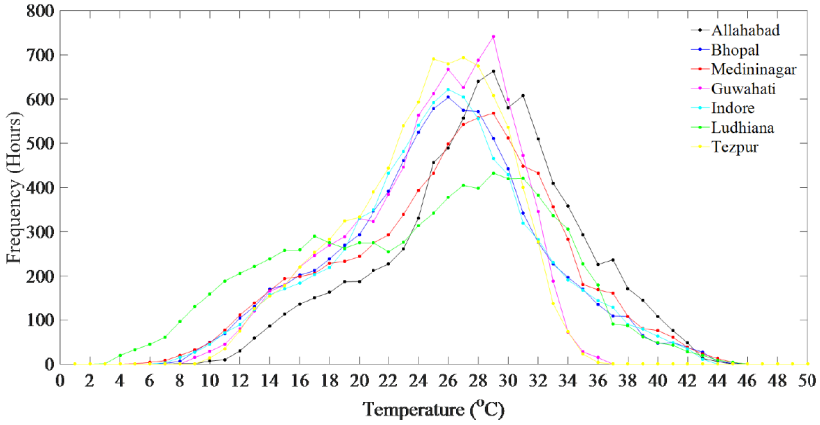

(C) Humid subtropical region

FIGURE 3.29: Temperature profiles of various cities in different climate regions of India plotted 113].

TABLE 3.4: Percentage of the annual time for which the temperature range persists in different cities in India.

Region / City	**Below** 25°C	25°C **to** 35°C	**Above** 35°C
Arid region			
Bikaner	40.9%	42.9%	16.2%
Bhuj	32.2%	56.4%	11.4%
Hisar	43.2%	41.9%	14.9%
Jaipur	41.4%	47.9%	10.7%
Jodhpur	40.0%	48.8%	11.2%
Semi-arid region			
Agra	40.5%	47.7%	11.8%
Aurangabad	44.2%	49.4%	6.4%
New Delhi	44.4%	47.0%	8.6%
Rajkot	32.5%	59.1%	8.4%
Tropical wet region			
Bhubaneshwar	28.0%	67.1%	4.9%
Cochin	22.8%	77.2%	0.0%
Goa	27.3%	72.6%	0.1%
Mangalore	28.7%	71.0%	0.3%
Tiruchirappalli	19.8%	73.3%	6.9%
Thiruvananthapuram	32.1%	67.9%	0.0%
Tropical wet and dry region			
Bengaluru	60.8%	38.8%	0.4%
Chennai	20.9%	72.6%	6.5%
Coimbatore	42.9%	56.1%	1.0%
Hyderabad	38.7%	54.1%	7.2%
Jamshedpur	35.5%	59.1%	5.4%
Kolkata	33.1%	63.9%	3.0%
Nagpur	35.1%	54.4%	10.5%
Mumbai	23.7%	75.4%	0.89%
Humid subtropical region			
Allahabad	29.9%	58.4%	11.8%
Bhopal	48.6%	44.7%	6.7%
Daltonganj	41.6%	50.0%	8.4%
Guwahati	49.3%	50.5%	0.2%
Indore	49.0%	44.2%	6.8%
Ludhiana	51.2%	42.3%	6.5%
Tezpur	53.1%	46.8%	0.05%

3.7.2 Development of numerical model with suitable control strategy

3.30) shows the schematic diagrams and representative P-h chart for the various ejector expansion systems. The dashed lines in schematics show alternate modes of operation depending upon control action, as ambient changes. Thermodynamic models for the various configurations are developed for a fixed cooling load of 10 kW particularly suitable for retail food refrigeration applications. The model for each system is developed using fundamental relations of conservation of mass, momentum, and energy for steady-state operation. The assumptions made for the development of numerical models are following:

- The kinetic energy of refrigerant is negligible at the inlet and exit of the ejector.
- In subcritical operation, the various ejector systems operate as EETRC.
- 16], the mixing occurs at evaporator pressure. In the constant pressure mixing model, the primary and secondary stream is assumed to be mixed at the same pressure (P_{evap}).
- 112 40]; 42]).
- Saturated vapor condition at the evaporator exit.
- The approach temperature of the air-cooled gas cooler is 2°C.
- vapor is subcooled by 5°C in the IHX before entering into the ejector motive nozzle.
- The refrigerant circulated through the second intercooler as shown in figure 4(c) is superheated by 5°C and its mass flow rate is set to 0.3 times of total mass flow in MCMIEETRC 41].
- For control, a transition mode is assumed in between subcritical operational mode and transcritical mode. 25°C ambient is selected as transition temperature with a dead band of ±1°C.
- Fan power consumption is 5% of the compressor power.

Total equivalent warming impact (TEWI) is computed as the sum of greenhouse effect from direct refrigerant (R744) release to the environment during the equipment's lifetime and indirect carbon emission from fossil fuel burnt for electricity consumed during its lifetime, Makhnatch 114],

$$TEWI = TEWI_{direct} + TEWI_{indirect}, \tag{3.63}$$

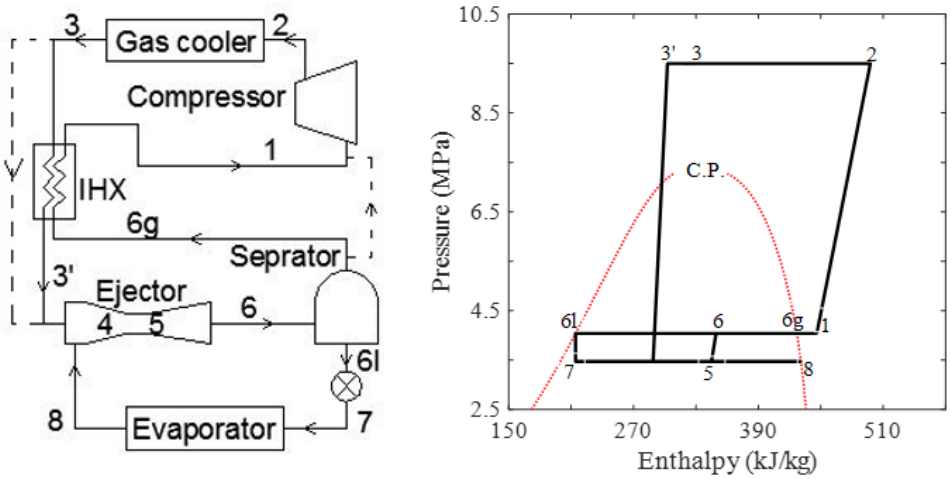

(A) EETRC+IHX

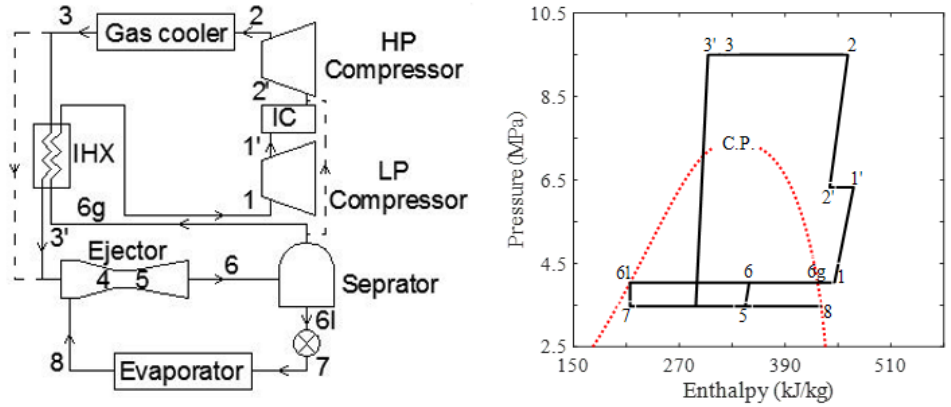

(B) MCEETRC+IHX

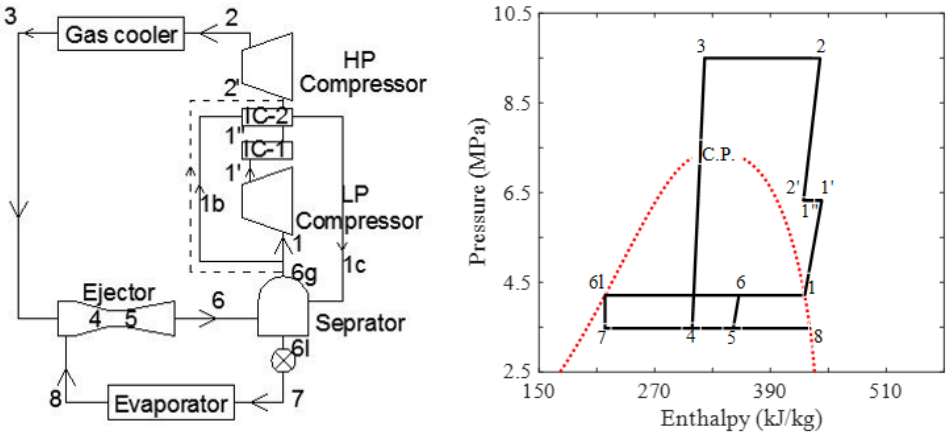

(C) MCMIEETRC

FIGURE 3.30: Various ejector expansion systems schematic and corresponding $P-h$ charts.

$$TEWI_{direct} = GWP \cdot L \cdot n + GWP \cdot m \cdot (1 - \alpha), \tag{3.64}$$

$$TEWI_{indirect} = E \cdot \beta \cdot n. \tag{3.65}$$

To calculate TEWI for various ejector systems, the following assumptions are made with reference 115]):

- The GWP of R744 is 1.
- The annual leakage rate is considered as 15% .
- The system operational lifetime is taken as 10 years.
- The R744 charge in ejector systems is set as 1 $kg_{R-744}kW_{cc}^{-1}$.
- The amount of refrigerant recycled is assumed as 95%.
- The amount of CO_2 emission due to electricity generation in the Indian context is set to 0.82 $kg_{CO_2}kWh^{-1}$ 116])

3.7.3 Numerical model for round the clock operation

For round the clock operation, the ambient may undergo considerable change within a day and across a season depending upon location. Therefore, the refrigeration system needs to be designed for operation under subcritical as well as supercritical mode. In order to obtain optimal performance, a suitable control strategy needs to be implemented for a smooth transition from one mode to the other. Our simulation showed that all the three ejector systems viz., EETRC+IHX, MCEETRC, and MCMIEETRC when operated in subcritical mode, runs similar to basic ejector expansion refrigeration system. In ambient temperature range 24°C to 26°C, the EETRC+IHX system runs in subcritical mode, while MCEETRC+IHX and MCMIEETRC run in transcritical mode. However, above 26°C, all the system runs under transcritical mode for better heat rejection in the gas cooler.

To maintain the heat rejection rate of refrigerant in gas cooler, a variable speed fan is recom- 117]. At lower ambient, a minimum heat rejection temperature is needed to be fixed due to the design limitation of condenser, it is termed as minimum condensing temperature. In the subcritical mode of operation, the minimum condensing temperature is assumed as 10° 118]) whereas the maximum condensing temperature is set to 31°C. In transition mode, the system needs to be operated carefully for maximization of COP, the transition temperature is assumed 25°C with a dead band of 1°C. Dead band is a range of particular input variables under which control system output is zero so that the system can be operated as per requirements. Entrainment ratio for the ejector, which is the ratio of suction to

TABLE 3.5: Component operating parameters and their control

Component	Parameter	Operating range
Evaporator	Evaporator temperature	Constant, -5 to -15°C
	Cooling capacity	10 kW
	Superheating	117]
Compressor	Speed control	Variable speed
Gas cooler / Condenser pressure	Supercritical pressure	7.5-12.5 MPa
	Subcritical pressure	Floating Dt=6K, Ge et al. 118]
	Minimum condensing temperature	10° 119]
	Gas cooler approach temperature	50° 117]
	Condenser subcooling	3° 117]
Ejector	Entrainment ratio	$X = M_p/(M_s + M_p)$
Transcritical / Subcritical cycle	Transition ambient temperature	25±1° 118]

motive mass flow rate, is assumed to be controlled by maintaining a particular vapor quality at 3.5.

3.7.4 Effect on system performance parameters under controlled operation

3.31) shows a comparative plot of change in operating parameters with a change in ambient temperature for a fixed evaporator temperature of -10°C for the various ejector cycles. 3.31(a). It is observed that energy consumption remains constant at low ambient, less than 10°C, since the minimum heat rejection pressure is fixed. The energy consumption, however, increases steadily during the subcritical mode of operation from 10°C ambient to 26°C. For the transcritical mode of operation that is beyond 26°C ambient, the energy consumption increases substantially. MCEETRC+IHX shows the lowest energy consumption for the almost entire range of operation. At very high ambient temperatures (44°C to 47°C), the energy consumption further increases where the performance of MCEETRC+IHX and MCMIEETRC are comparable.

3.31(b). As the minimum heat rejection pressure is fixed for lower ambient temperature, the COP of the system remains more or less constant for lower temperature range but it gradually decreases with an increase in ambient temperature. In the transcritical mode of operation, MCEETRC+IHX shows higher COP among all the ejector systems up to 40° C. However, the COP advantage of MCEETRC+IHX compared to MCMIEETRC diminishes above 40°C ambient because MCMIEETRC consumes comparatively less compressor power at high temperature due to second stage intercooling. While EETRC+IHX shows the lowest COP in transcritical mode.

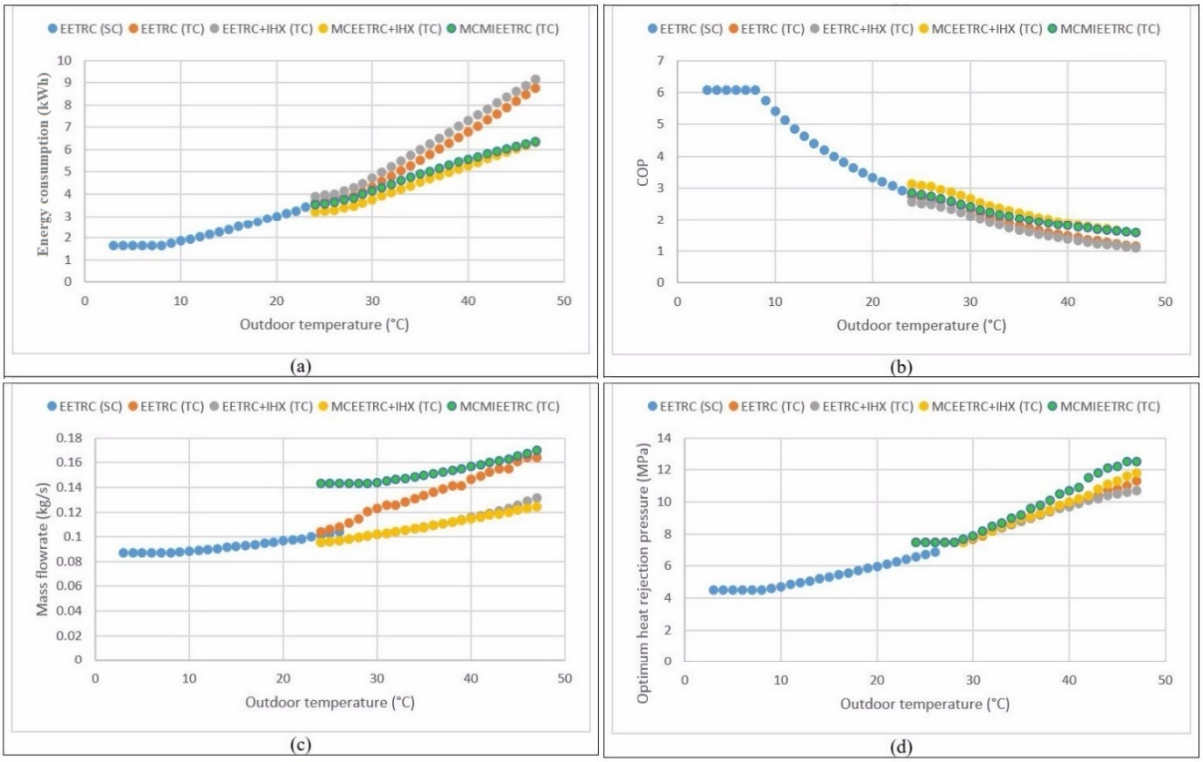

FIGURE 3.31: Comparison of system performance parameters at various ambient temperatures.

3.31(c) represents the variation of the refrigerant mass flow rate against ambient temperature. It is observed that the required mass flow rate in the system increases with an increase in ambient temperature for all configurations to meet the fixed cooling capacity. Further, in transcritical mode, the mass flow rate required in MCMIEETRC is higher than any other ejector system. This is because, in MCMIEETRC, the additional refrigerant is required for intercooling. The overall system mass flow rate for EETRC and EETRC+IHX is comparable. It is also observed that during transcritical operation, the mass flow rate is sensitive to gas cooler pressure, the same is identified for further exploration.

3.31 (d) shows the variation of optimum gas cooler pressure concerning ambient temperature. At the onset of transcritical operation, just below 25°C ambient, the optimum heat rejection pressure is 7.5 MPa and remains constant in the transition zone. Thereafter the pressure

steadily increases. The highest operating pressure is kept limited to 12 MPa, in view of design constraints. EETRC+IHX system exhibits the lowest optimum gas cooler pressure whereas MCMIEETRC shows the highest optimum gas cooler pressure for the range of operation.

3.7.5 Annual energy consumption for various cities under controlled operation

The annual energy consumption for various ejector systems employing the control strategy discussed earlier is compiled based on year around environmental data for the selected cities and 3.32).

From the analysis, the following observations are made:

- Annual energy consumption increases as evaporator temperature decreases.
- MCEETRC+IHX consumes the least annual energy followed by EETRC, MCMIEETRC, and EETRC+IHX.
- Performance of MCMIEETRC and EETRC+IHX configurations are found similar for the weather condition of arid and semi-arid regions.
- For weather conditions of tropical wet, tropical wet and dry, and humid subtropicals regions, MCMIEETRC, EETRC+IHX, and EETRC have comparable performance.

3.7.6 Impact on TEWI for various cities under controlled operation

3.33 3.62 3.63 3.64) for various ejector systems evaluated for 30 different cities for year-round operation and three different evaporator temperatures. The following conclusions are drawn from the study.

- TEWI increases with a decrease in evaporator temperature, the same is due to a hike in the amount of energy consumption.
- Overall lowest TEWI is recorded in the humid subtropical region, the same is found lowest for the MCEETRC+IHX.
- EETRC, EETRC+IHX, and MCEETRC+IHX configurations are found to have lower TEWI in the humid subtropical region. While in the Tropical wet region, MCMIEETRC gives lower TEWI.

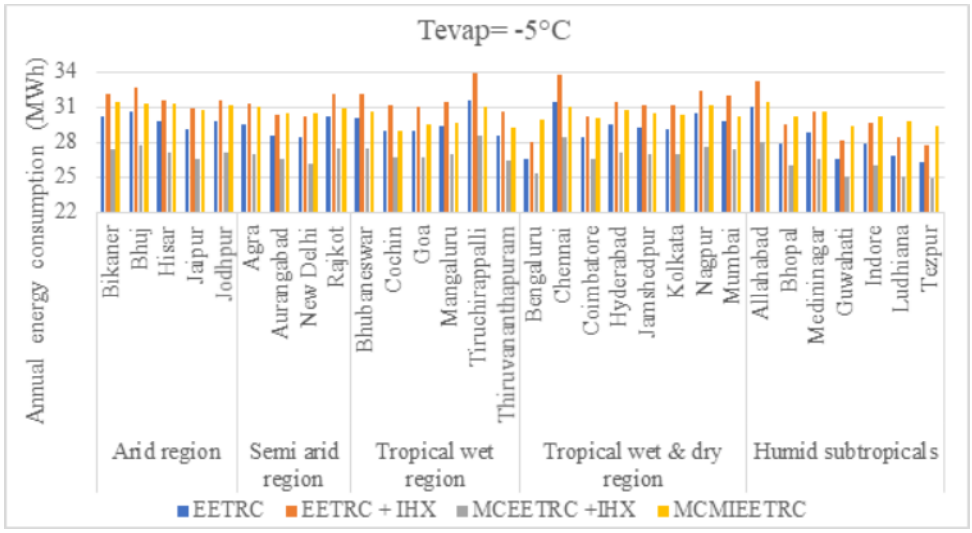

(A)

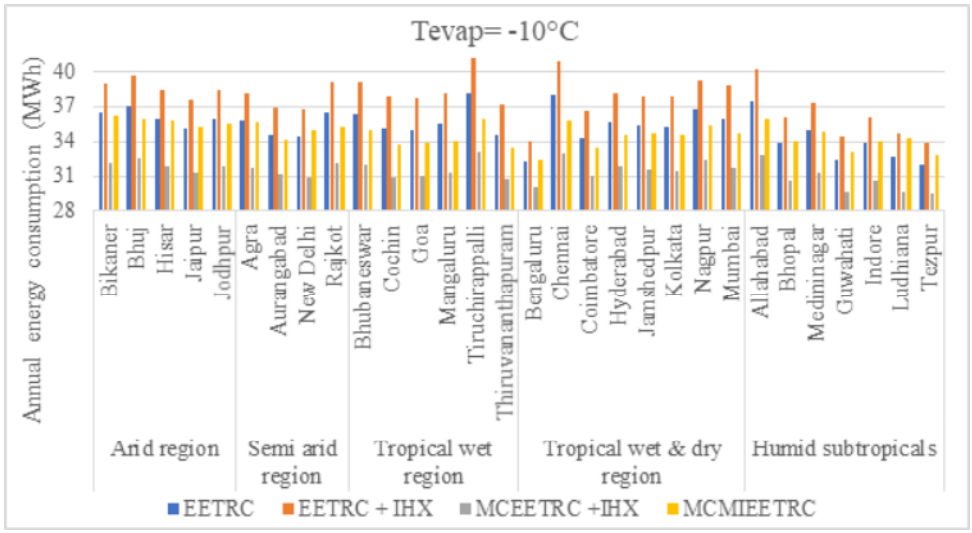

(B)

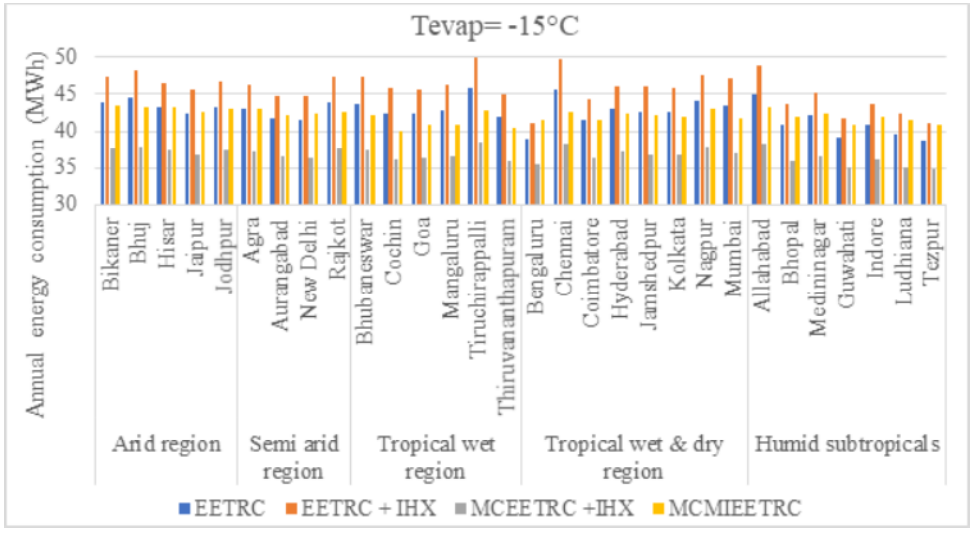

(C)

FIGURE 3.32: Comparison of annual energy consumption for various cities at different evaporator temperatures.

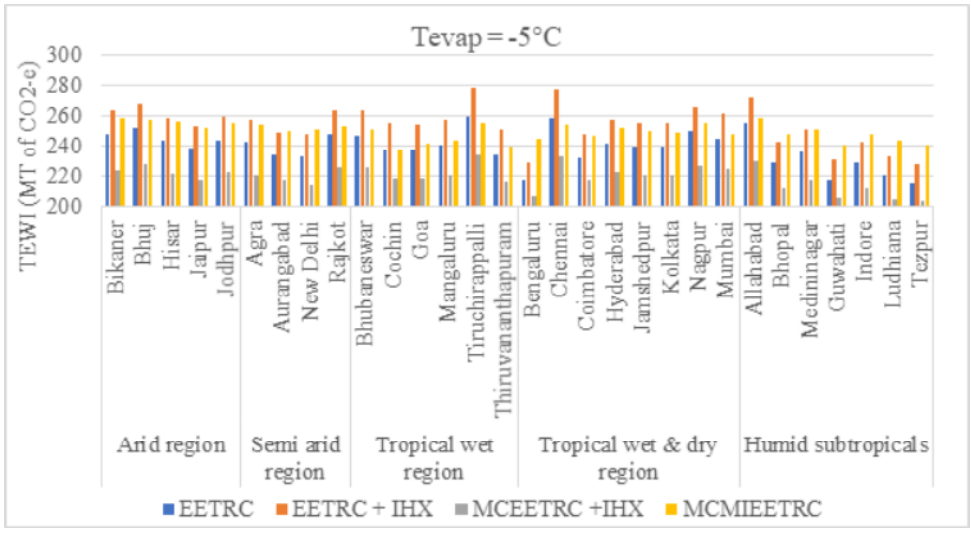

(A)

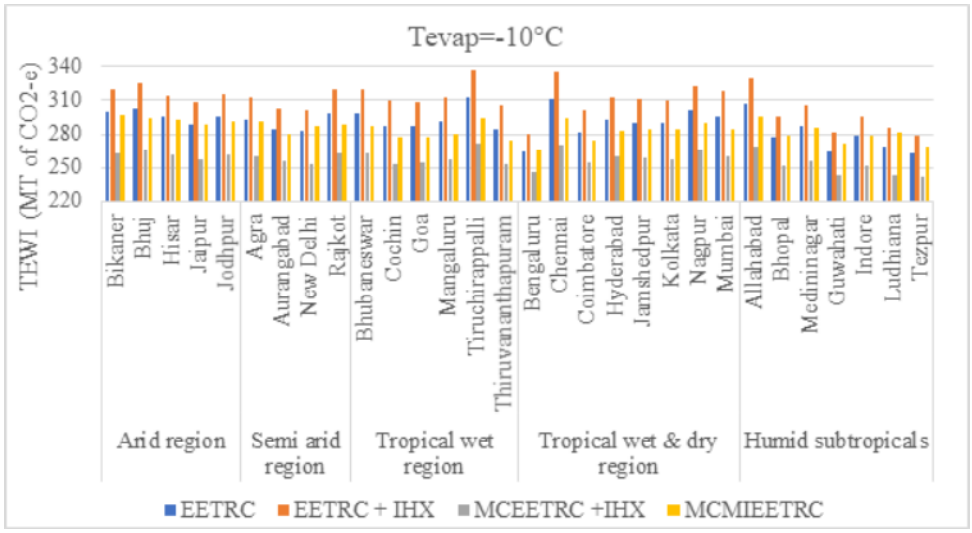

(B)

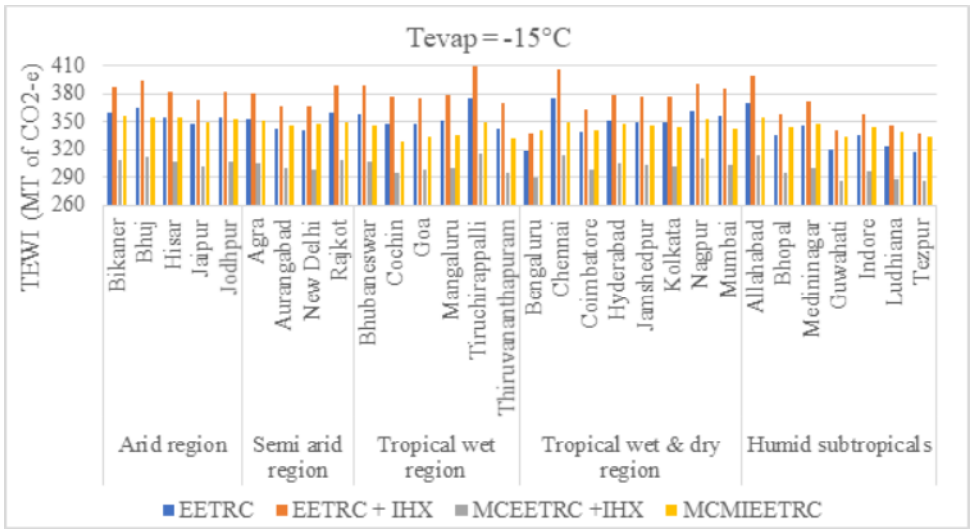

(C)

FIGURE 3.33: Comparison of TEWI for various cities at different evaporator temperatures.

3.8 Multi Ejector Refrigeration System

Here a modification in the DERC system is proposed to utilize the exergy during the expansion process. Expansion valve EP2 of DERC is replaced with a work recovery expander (WRE), which compensates for some amount of the compression work. A DERC is conceived having one compressor, one gas-cooler, one internal heat exchanger, one lower temperature evaporator, one medium temperature evaporator, one liquid vapor separator, two expansion valves, and two 3.34). In the modified dual ejector refrigeration system, the expansion valve (EP2) is replaced by a work recovery expander which utilizes the expansion exergy.

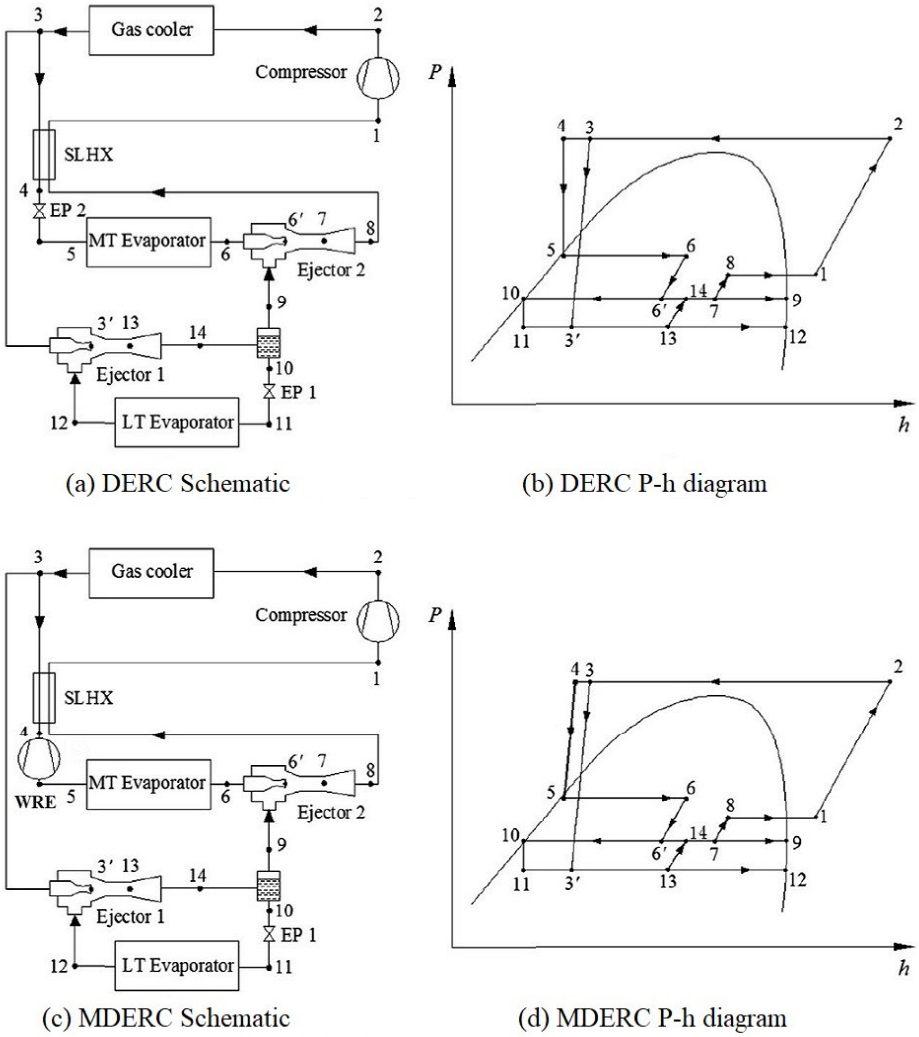

FIGURE 3.34: Schematics and $P-h$ diagrams of MDERC and DERC.

3.34 (a,b) illustrates the schematic and corresponding $P-h$ chart of DERC and while 3.34 (c,d) present the schematic and $P-h$ chart of a modified dual ejector refrigeration cycle (MDERC).

DERC and MDERC are investigated separately based on the following assumptions:

- Steady-state operation.
- Fully insulated Ejectors.
- Kinetic energies of refrigerants neglected at ejector inlet and outlet.
- Motive nozzle, mixing process, and diffuser working process efficiencies remain constant, 62],

  17])
- Constant pressure mixing in the ejector.
- 55], Ksayer and

  58]).
- Refrigeration capacity ratio (ϕ) taken as 1.

The thermodynamic model of the DERC and MDERC are developed using thermodynamic 3.66 3.87). The simulation program is developed in MATLAB (R2016a). State properties of refrigerants are computed using REFPROP version 9.0.

3.8.1 Energy based investigation

For compressor in a single compressor cycle, the power consumption per unit mass of the mixture is given by

$$W_c = m_1(h_2 - h_1) = \frac{m_1(h_2 - h_1)}{\eta_c}. \tag{3.66}$$

7])

$$\eta_c = 0.815 + 0.022\left(\frac{P_2}{P_1}\right) - 0.0041\left(\frac{P_2}{P_1}\right)^2 + 0.0001\left(\frac{P_2}{P_1}\right)^3. \tag{3.67}$$

The heat transfer in the gas cooler is given by

$$Q_{gc} = m_2(h_2 - h_3). \tag{3.68}$$

The heat transfer rate per unit mixed mass flow rate is given by

$$Q_{gc} = m_2(h_2 - h_3). \tag{3.69}$$

The energy balance in the internal heat exchanger is given by

$$m_{p2}(h_3 - h_4) = (m_{p1} + m_{p2})(h_1 - h_8). \tag{3.70}$$

For the ejector, the different relations used are

$$\eta_m = \sqrt{2\eta_m(h_{mi} - h_{mi\cdot is\cdot o})x1000}, \tag{3.71}$$

$$V_{mix} = \frac{V_{m\cdot o}}{1+u}\sqrt{\eta_{mix}}, \tag{3.72}$$

$$h_{d,i} = \frac{h_{m,i} + h_{s,i}}{1+u} - \frac{V_{mix}^2}{1000}, \tag{3.73}$$

$$h_{d,o} = \frac{h_{m,i} + uh_{s,i}}{1+u}, \tag{3.74}$$

and finally,

$$h_{d\cdot is\cdot o} = h_{d,i} + (h_{d,o} - h_{d,i})\eta_d. \tag{3.75}$$

For the expansion / control valves, the energy balance is given by

$$\text{For expansion valve 1} : h_{11} = h_{10}, \tag{3.76}$$

$$\text{For expansion valve 2} : h_5 = h_4. \tag{3.77}$$

For evaporators, the cooling capacity per unit mixture mass flow rate is given by

$$Q_{MT,evap} = m_{p2}(h_6 - h_5), \tag{3.78}$$

$$Q_{LT,evap} = m_{s1}(h_{12} - h_{11}). \tag{3.79}$$

The total cooling capacity of the system is given by

$$Q_{total} = Q_{MT,evap} + Q_{LT,evap}. \tag{3.80}$$

Entrainment ratio (u) and pressure recovery ratio (PRR) are considered as important parameters to assess ejector performance. The entrainment ratio is defined as the ratio of suction mass flow rate to motive mass flow rate. While the ratio of pressure at ejector exit to inlet pressure of ejector suction flow is termed as pressure recovery ratio. In the simulation program, the entrainment ratio of each ejector is defined as:

$$u_1 = \frac{m_{12}}{m_{3'}} \text{ and } u_2 = \frac{m_9}{m_6} \tag{3.81}$$

The relationship between refrigerant mixture quality (ξ_{14}) at ejector 1 outlet and ejector 1 entrainment ratio (u_1) is expressed as:

$$\xi_{14} = \frac{1}{1+u_1}. \tag{3.82}$$

The pressure ratios of each ejector and total pressure recovery ratio for the cascade ejector are defined as:

$$PRR_1 = \frac{P_{14}}{P_{12}}, \quad PRR_2 = \frac{P_8}{P_9} \tag{3.83}$$

$$PRR_{total} = PRR_1 \times PRR_2 = \frac{P_8}{P_{12}} \tag{3.84}$$

The refrigeration capacity ratio (ϕ) is defined as,

$$\phi = \frac{Q_{MT}}{Q_{LT}} = \frac{(1-\beta)(h_6 - h_5)}{\beta u_1 (h_{12} - h_{11})} = \frac{(1-\beta)\xi_{14}(h_6 - h_5)}{\beta(1-\xi)(h_{12} - h_{11})} \tag{3.85}$$

Here, β is the ratio of mass flow rates of the two motive streams of the ejectors. The same is introduced to identify the effect of refrigeration capacity allocation between MT and LT evaporators. β can be defined as:

$$\beta = \frac{m_{p1}}{m_{p1} + m_{p2}} = \frac{u_2}{1 + u_2}. \tag{3.86}$$

The COP and second law efficiency of the system can be calculated as:

$$COP = \frac{Q_t}{W_c} \text{ and } \eta_{IInd} = 1 - \frac{I_t}{W_c}. \tag{3.87}$$

3.8.2 Impact on COP

3.35) shows the system performance for a range of gas cooler exit pressure within range (8 MPa to 12 MPa) at various gas cooler exit temperatures (T_{gco}= 35, 40, 45, 50) for DERC and MDERC.

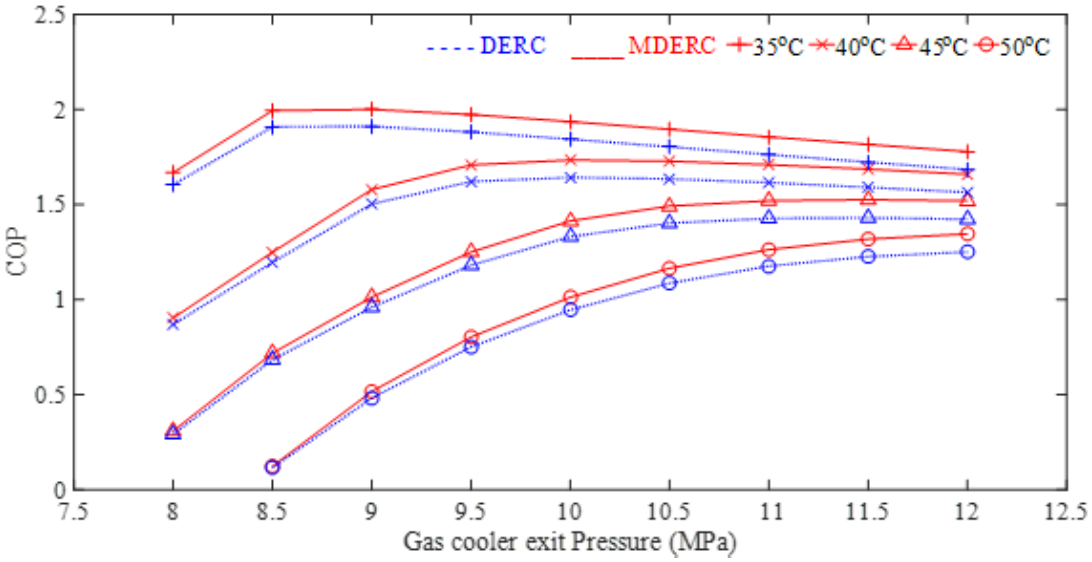

FIGURE 3.35: Effect of gas cooler exit pressure on system performance.

3.35), that MDERC gives better system performance in terms of COP. The same is more prominent at higher T_{gco} and P_{gco}. It is because MDERC utilizes the exergy during the expansion process, the extent of the same is found higher at elevated gas cooler exit temperature and gas cooler exit pressure. Compared to DERC, MDERC has 4.7% to 7.6% higher COP. Further, for lower gas cooler exit temperature (35°C and 40°C), the COP is observed to have an incremental trend concerning the increase in P_{gco}. While, for higher T_{gco}, COP increases with pressure up to a maximum value, and then steadily decreases with an increase in gas cooler exit pressure due to obvious reasons.

3.8.3 Effect on ejector performance

Ejector performance mainly depends upon two parameters namely pressure ratio and entrainment 3.36) depicts the variation in pressure ratio and entrainment ratio concerning gas cooler exit pressure. The entrainment ratio show overall increasing trend with an increase in the gas cooler exit pressure for a fixed gas cooler exit temperature ($T_{gco} = 40$°C) and evaporator temperatures ($TMT = 0$°C; $TLT = -25$°C). It can be explained as following: at higher gas cooler exit pressure, higher energy is available at the inlet of the motive nozzle which in turn leads to a higher suction mass flow rate of the ejector. Further, the pressure ratio is observed to decrease rapidly with an increase in gas cooler exit pressure and then flatten out. It happens since the pressure ratio is inversely proportional to the entrainment ratio. Furthermore, in both MDERC and DERC, the inlet conditions at the ejectors are almost the same. There is no significant difference is observed in the overall performance of the two ejectors for both the cycle configurations.

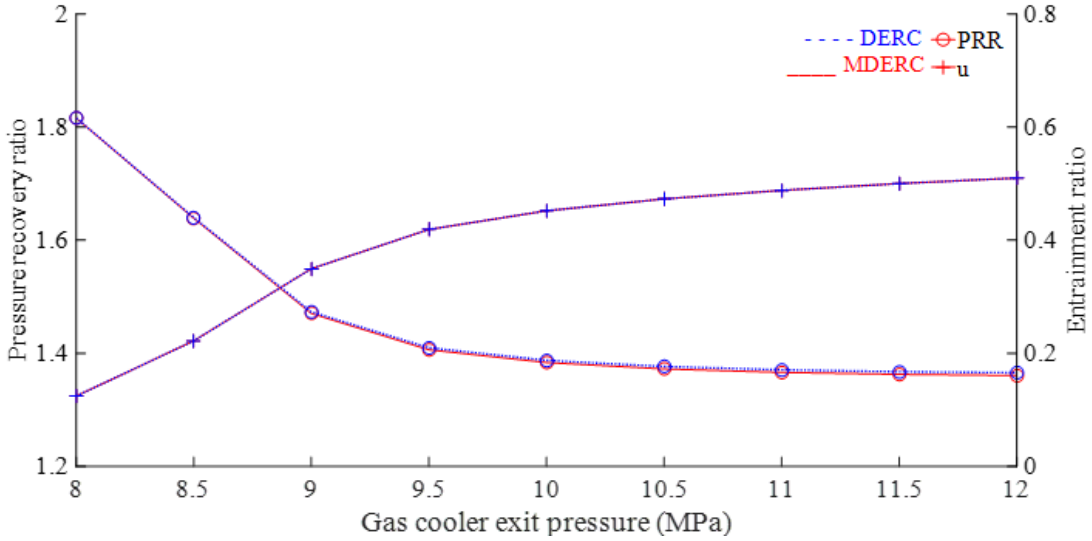

FIGURE 3.36: Effect of gas cooler exit pressure on pressure recovery ratio and entrainment ratio.

3.8.4 Effect of the lower temperature evaporator on system performance

3.37) shows the effect of LT evaporator temperature on the system performance at fixed inlet condition of the motive nozzle (P_{gco} = 9 MPa; T_{gco} = 35°C) and MT evaporation temperature (TMT = 0°C). COP and second law efficiency both are observed to have a higher value for MDERC compared to DERC. COP for MDERC is about 3.7 % to 6% higher while second law efficiency is about 2.1% to 4.5% higher for the full range of TLT operation. Further, COP for both the systems shows an incremental trend for an increase in TLT due to obvious reasons. Furthermore, second law efficiency for both the systems shows an overall constant trend. Therefore, it can be concluded that the system second law efficiency is not sensitive to the variation of the LT evaporator temperature.

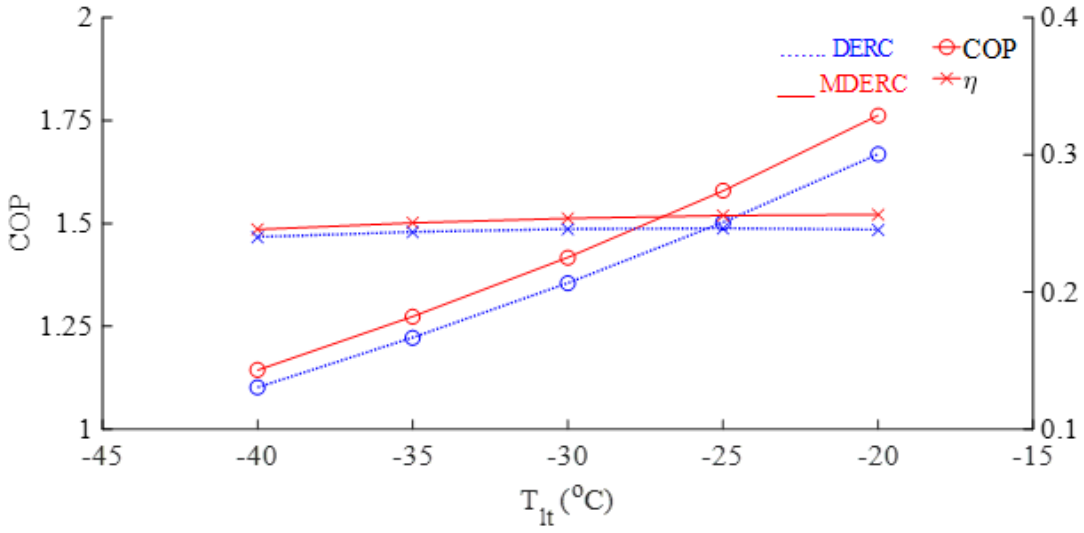

FIGURE 3.37: Effect of lower temperature evaporator on system performance.

3.8.5 Effect of lower temperature evaporator on ejector performance

3.38) shows the effect of lower temperature evaporator on the performance of ejector-2 for fixed inlet condition of motive nozzle (P_{gco} = 9 MPa; T_{gco} = 35°C) and MT evaporation temperature (TMT = 0°C). It shows a slight increment in the entrainment ratio with an increase in LT evaporation temperature. It can be explained as when LT evaporation temperature decreases, the evaporation pressure also decreases which leads to increment in enthalpy difference in the evaporator. Further, refrigerant quality at the ejector-1 outlet would decrease with a decrease in LT evaporation temperature. It tends to increase the mass flow rate in the LT evaporator to meet the fixed refrigeration capacity ratio. Further entrainment ratio of MDERC is observed to be higher compared to DERC.

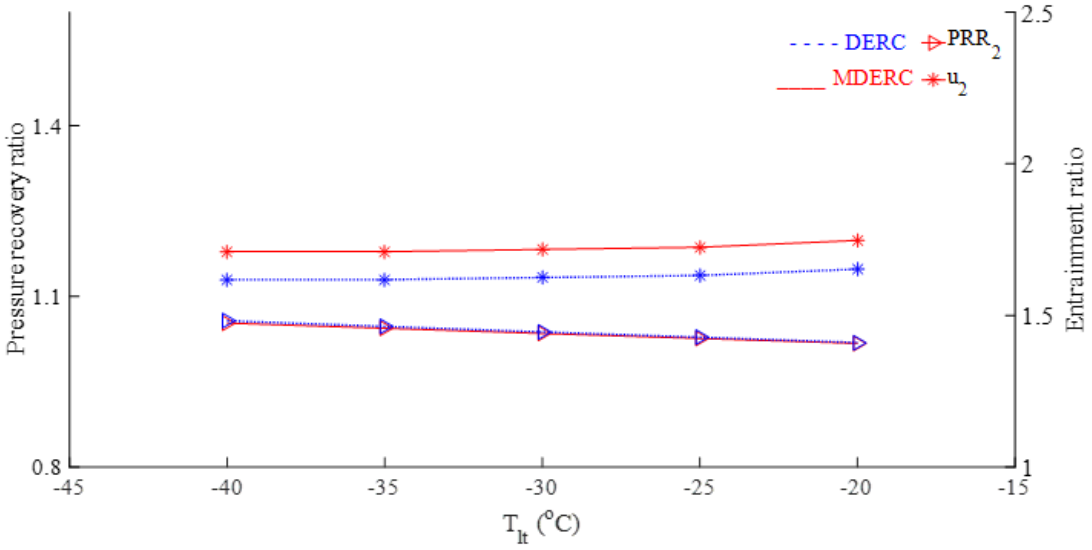

FIGURE 3.38: Effect of lower temperature evaporator on ejector performance.

3.8.6 Exergy destruction

For each component of the different cycle configurations, the exergy destruction rate per unit mass flow rate through various components are expressed by the following equations: For the compressor, the exergy destruction is given by

$$I_c = T_0(S_2 - S_1). \tag{3.88}$$

For the gas cooler, the exergy destruction is given by

$$I_{gc} = m_2((h_2 - h_3) - T_0(S_2 - S_3)). \tag{3.89}$$

For the ejectors, the exergy destruction is given by

$$I_{ejec,1} = T_0(m_{14}(1 + U_1)S_{14} - m_3S_3 - m_{12}S_{12}), \tag{3.90}$$

$$I_{ejec,2} = T_0(m_8(1 + U_2)S_8 - m_6S_6 - m_9S_9). \tag{3.91}$$

For the evaporators, the exergy destruction is given by

$$I_{MT,evap} = m_6\left(T_0(S_6 - S_5) - (h_6 - h_5)\frac{T_0}{T_{ref,2}}\right), \tag{3.92}$$

$$I_{LT,evap} = m_6\left(T_0(S_{12} - S_{11}) - (h_{12} - h_{11})\frac{T_0}{T_{ref,1}}\right). \tag{3.93}$$

For the expansion / control valves, the exergy destruction is given by

$$I_{exp,1} = T_0 m_{11}(S_{11} - S_{10}), \tag{3.94}$$

$$I_{exp,2} = T_0 m_4(S_5 - S_4). \tag{3.95}$$

The total exergy destruction of the cycle is the sum of individual component exergy destruction rates

$$I_{total} = I_c + I_{gc} + I_{ejec} + I_{exp} + I_{evap}. \tag{3.96}$$

The overall exergy balance for the cycle is given by

$$W_c = W_{rev} + I_{total}. \tag{3.97}$$

The second law efficiency for each cycle is

$$\eta_{IInd} = \frac{W_{rev}}{W_c}. \tag{3.98}$$

3.39) shows the component-wise exergy destruction as well as total exergy destruction for MDERC and DERC. MDERC has total exergy destruction of 57.33 kJ/kg·K while the same is about 60.17 kJ/kg·K for DERC. The highest exergy destruction is observed in the gas cooler, which is about 39.1 % of the total exergy destruction of MDERC and about 37.1 % of the total exergy destruction of DERC followed by ejectors and compressor. The WRE significantly utilizes the exergy available during the expansion process. The same is highlighted in the figure. The WRE has 85 % lesser exergy destruction in comparison to Exp 2 used in DERC.

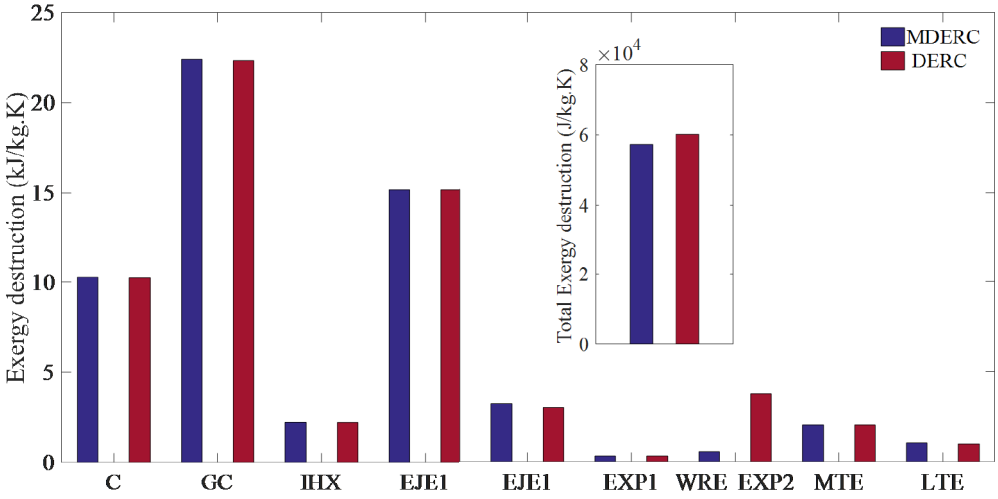

FIGURE 3.39: Component wise exergy destruction of MDERC and DERC.

TABLE 3.6: 120].

Property	R-744	R-744A	Inference about R-744A
Molecular weight (kg/kmol)	44.01	44.013	–
Critical pressure (MPa)	7.377	7.245	Lower heat rejection pressure
Critical temperature (°C)	31.1	36.4	Moderately warm weather operation
Boiling point (°C)	-78.4	-88.47	Ensures single phase at evaporator exit
Tripple point temperature (°C)	-56.55	-90.82	Lower evaporator temperature operation
Toxicity (ppm)	5000	1000	Low toxicity
GWP	1	265	Higher GWP
ODP	0	0.017	Nearly similar
Latent heat of vap. (kJ/kg)	574	374.28	Higher mass of ref. in evaporator

3.9 Comparison of R-744 and R-744A Ejector Refrigeration System

The critical temperature of R744 and R744A is 31.1°C and 36.4°C respectively, they require higher heat rejection pressure for maximizing COP, compared to conventional refrigerants in warm weather conditions. Because of high operating pressure, large expansion losses typically occur during expansion from the supercritical region to the subcritical region through the throttling valve. R744A has properties similar to R744 and both have high heat rejection 3.6 presents the properties of R744 and R744A and comparative inferences about R744A.

3.9.1 Comparison based on performance parameters: Single ejector system

Simulation for EETRC is developed in MATLAB. State properties of the refrigerants are 3.40) shows the variation of COP for various gas cooler exit pressure for R744 and R744A at three different gas cooler exit temperatures keeping evaporator temperature constant at 5°C. COP for both R744 and R744A cycle is observed to reach a maximum value at lower gas cooler exit pressure and then decreases with an increase in pressure. This can be explained as at higher gas cooler exit pressure and temperature, vapor quality at ejector exit is also higher which in turn leads to a higher mass flow rate handled by a compressor. It is also concluded that R-744A has lower optimum gas cooler exit pressure compared to R-744. However, it is observed that the R744A ejector cycle gives comparatively better performance at gas cooler pressure below 8.5 MPa, 9.5 MPa, and 10.5 MPa for gas cooler exit temperature 35°C, 40°C and 45°C respectively. The maximum COP obtainable of R744A EETRC is 10.13 % higher than the maximum COP of R744 EETRC.

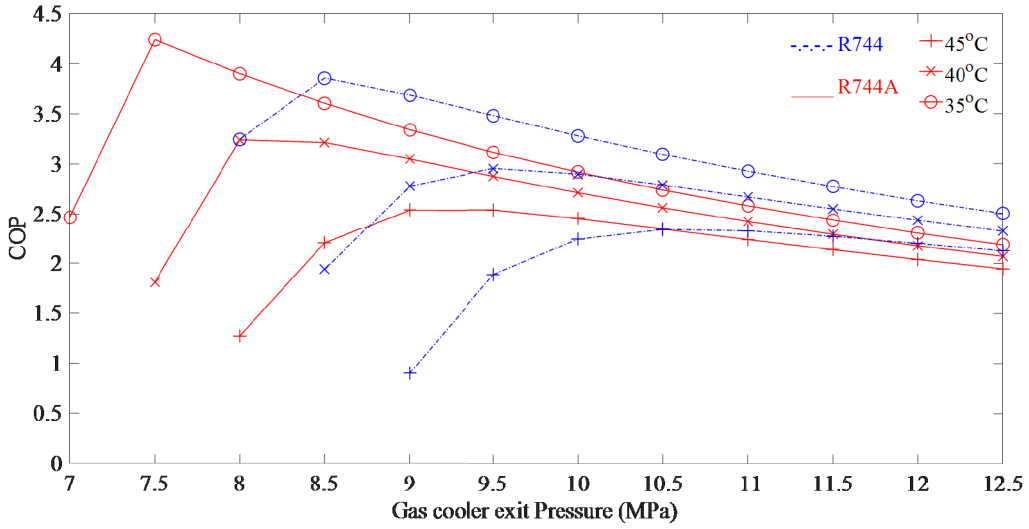

FIGURE 3.40: Effect of gas cooler exit temperature on cycle performance.

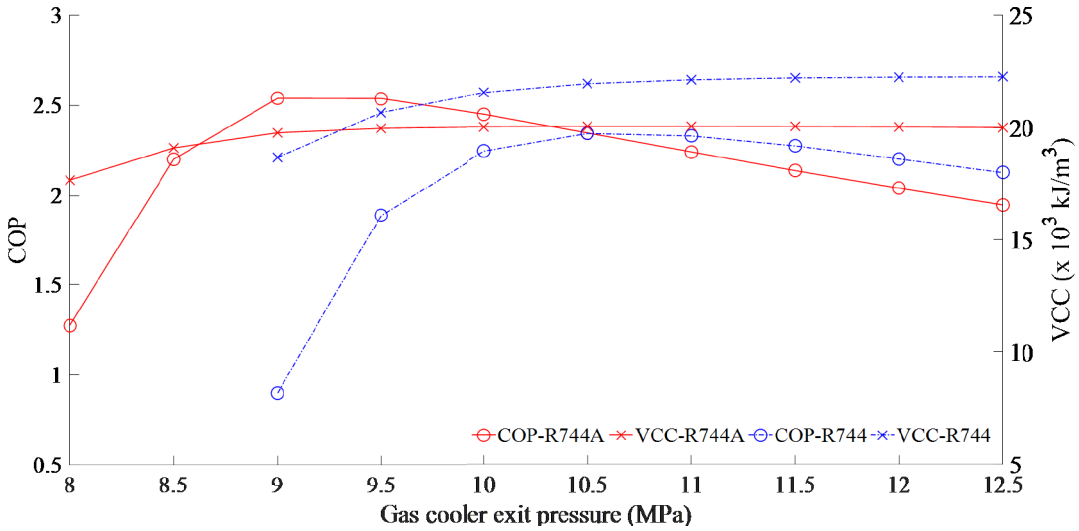

FIGURE 3.41: Effect of gas cooler exit pressure on cycle performance.

3.41) exhibits the effect of the gas cooler exit pressure on cycle performance parameters (COP and VCC) at fixed gas cooler exit temperature and evaporator temperature. It is noted that COP of R744A EETRC is higher than R744 EETRC at gas cooler exit pressure below 10.5 MPa. A slight increment in volumetric cooling capacity (VCC) is observed at lower gas cooler exit pressure for R744A. VCC of R744A is found higher than R744 at the gas cooler exit pressure below about 9.3 MPa which in turn helps to have higher COP at lower gas cooler exit pressure. At higher gas cooler exit pressure however, the R744A ejector cycle will require more mass of refrigerant in evaporator compared to the R-744 ejector cycle. The maximum cooling capacity of R744 EETRC and R744A EETRC is 22.26 MJ/m^3(12.5 MPa) and 20.07 MJ/m^3 (11 MPa) respectively.

Variation in ejector performance concerning gas cooler exit pressure is expressed in terms of 3.42). It is observed that with an increase in the gas cooler exit pressure, PRR decreases whereas ER increases, and beyond about 11 MPa pressure, there is very little change with further increase in gas cooler exit pressure. A possible explanation is that, at higher gas cooler pressure, the pressure energy available at motive nozzle is also higher which in turn leads to higher entrainment ratio. R744A EETRC shows higher ER while R744 EETRC shows higher PRR for the entire range of operation.

From the above discussion, it is concluded that the volumetric cooling capacity for both the refrigerants does not vary much with an increase in gas cooler pressure but the entrainment ratio varies significantly. This means although the mass flow rate in the evaporator remains almost constant with an increase in gas cooler exit pressure, yet there is a decrease in motive nozzle mass flow rate, which reflects a decrease in the total system mass flow rate. In order to compare the performance of two refrigerants, the system mass flow rate is an important criterion.

3.7 shows the computed system mass flow rate for various operating conditions for a 10 kW refrigeration system.

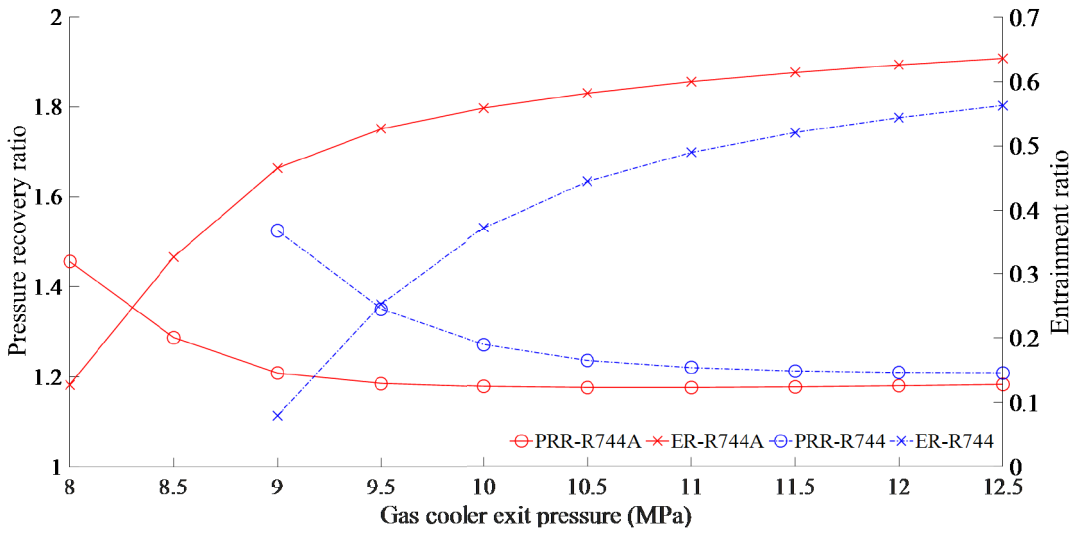

FIGURE 3.42: Effect of gas cooler exit pressure on ejector performance.

It can be concluded that at maximum COP condition, R744A EETRC requires less overall mass 3.43) shows the effect of evaporator temperature on the cycle performance parameters at a fixed inlet condition of the motive nozzle (P_{gco} = 10.5 MPa and T_{gco} = 45°C). It is observed that COP for both cycles increases with an increase in evaporator temperature. Although there is a decrement in RE and Wc with increment in evaporator temperature yet the decrement in compressor work is more prominent. COP of R744A EETRC is lesser compared to R744 EETRC at lower evaporator temperature. Both

TABLE 3.7: System mass flow rate required at optimum operating conditions (maximum COP) for the R-744A and the R-744 EETRC system

	T_{gco} = 35° C		T_{gco} = 40° C		T_{gco} = 45° C	
$P_{gco}(MPa)$	R-744A (kg/s)	R-744 (kg/s)	R-744A (kg/s)	R-744 (kg/s)	R-744A (kg/s)	R-744 (kg/s)
7.5	0.120957*	0.744079	0.348826	–	0.613258	–
8.0	0.118198	0.188299	0.144636*	–	0.489854	–
8.5	0.116435	0.135647*	0.131148	0.328854	0.209280	–
9.0	0.115302	0.128887	0.126591	0.180172	0.156592*	0.659488
9.5	0.114425	0.125473	0.124118	0.150918*	0.142776	0.27299
10.0	0.11368	0.123358	0.122329	0.14131	0.136808	0.195024
10.5	0.113156	0.121854	0.121005	0.136325	0.133197	0.156685*
11.0	0.112646	0.120657	0.119978	0.13312	0.130663	0.149877
11.5	0.112244	0.119735	0.119221	0.130905	0.128882	0.145487
12.0	0.111946	0.119065	0.118602	0.129249	0.127478	0.142237
12.5	0.111654	0.118416	0.118000	0.127949	0.12641	0.659488

cycles approach towards equal COP at higher evaporator temperature. It can be ascribed to the fact that at lower evaporator temperature the difference, $W_{c,R744A} - W_{c,R744}$, is higher.

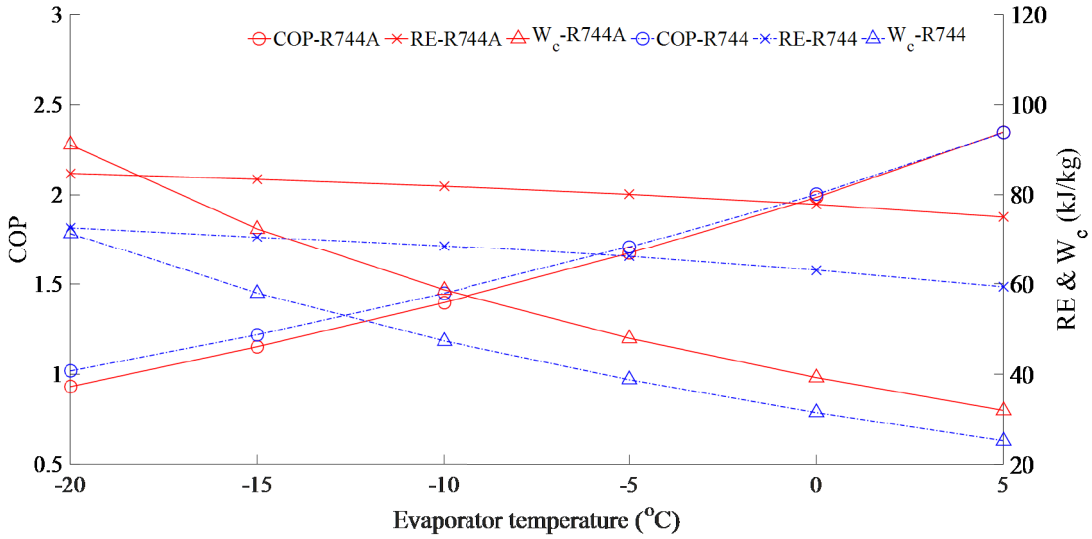

FIGURE 3.43: Effect of evaporator temperature on cycle performance.

3.44) shows the effect of evaporator temperature on ejector performance for both the refrigerants keeping motive nozzle inlet condition (P_{gco}=10.5 MPa and T_{gco}=45°C) constant. It is observed that PRR decreases while ER increases as evaporator temperature increases. At lower evaporator temperature and pressure, the difference in pressure of motive nozzle inlet and outlet is much higher, this leads ejector to gain higher pressure recovery and lower ER. Overall, it can be concluded that ER is higher whereas PRR is lower for R744A EETRC compared to R744 EETRC for the entire range of operation.

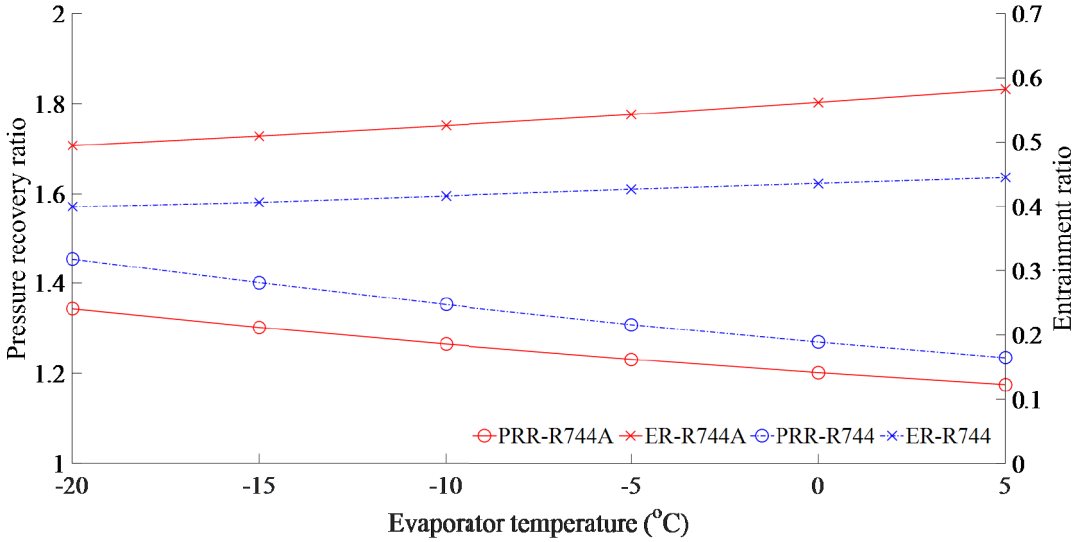

FIGURE 3.44: Effect of evaporator temperature on ejector performance.

3.9.2 Comparison based on performance parameters: Multi ejector system

A DERC is conceived having one compressor, one gas-cooler, one internal heat exchanger, one lower temperature evaporator, one medium temperature evaporator, one liquid vapor separator, 3.34 (a). DERC is investigated for two refrigerants (R744A and R744) separately based on the following assumptions:

- Steady-state operation.
- Fully insulated Ejectors.
- Kinetic energies of refrigerants neglected at ejector inlet and outlet.
- Motive nozzle, mixing process, and diffuser working process efficiencies remain constant, 62], 17])
- Constant pressure mixing in the ejector.
- 55], Ksayer and 58]).
- Refrigeration capacity ratio (ϕ) taken as 1.

The thermodynamic model of the DERC is developed using basic conservation relations as 3.66 3.87). The simulation program is developed in MATLAB (R2016a). State properties of refrigerants are computed using REFPROP version 9.0. The various system

performance parameters for the dual temperature cascade ejector R744A cycle are compared to its counterpart R744 cycle.

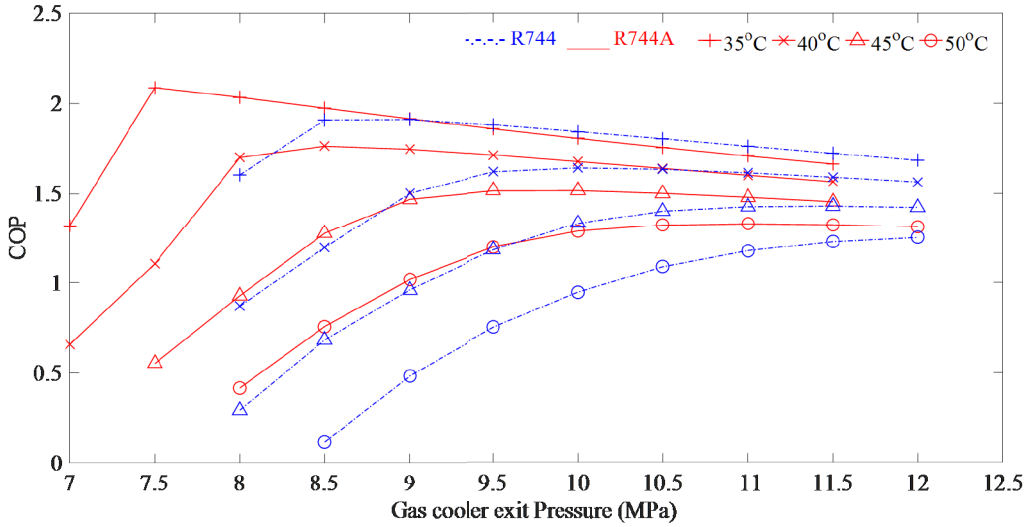

FIGURE 3.45: COP versus P_{gco} at various T_{gco}.

3.45) shows the comparative performance of R744 and R744A system at various gas cooler exit temperature for a range of gas cooler pressure (7 MPa to 12 MPa). System performance is observed to degrades with the rise in gas cooler heat rejection temperature due to obvious reasons for both the refrigerants. Both refrigerants have their optimal heat rejection pressure at each gas cooler heat rejection temperature. At lower T_{gco} the heat rejection pressure of gas cooler is observed to be lower, the same increase with an increase in T_{gco}. For selected T_{gco}, the R744A system is observed to have higher system performance. The R744A system, in comparison to the R744 system, shows lower heat rejection pressure for identical operating T_{gco}. Compared to the system using R744, the R744A system is found to have 6.08% to 8.9% higher COP for selected operating conditions. Ejector performance mainly depends on two parameters namely

3.46) depicts the variation in pressure ratio and entrainment ratio concerning gas cooler exit pressure. The entrainment ratio shows an overall increasing trend with the increase in the gas cooler exit pressure for a fixed gas cooler exit temperature ($T_{gco} = 40°C$) and evaporator temperatures ($T_{MT} = 0°C$; $T_{LT} = -25°C$). It can be explained as following: at higher gas cooler exit pressure, higher energy is available at the inlet of the motive nozzle which in turn leads to a higher suction mass flow rate of the ejector. Further, the pressure ratio is observed to decrease rapidly with an increase in gas cooler exit pressure and then flatten out. It is because the pressure ratio is inversely proportional to the entrainment ratio.

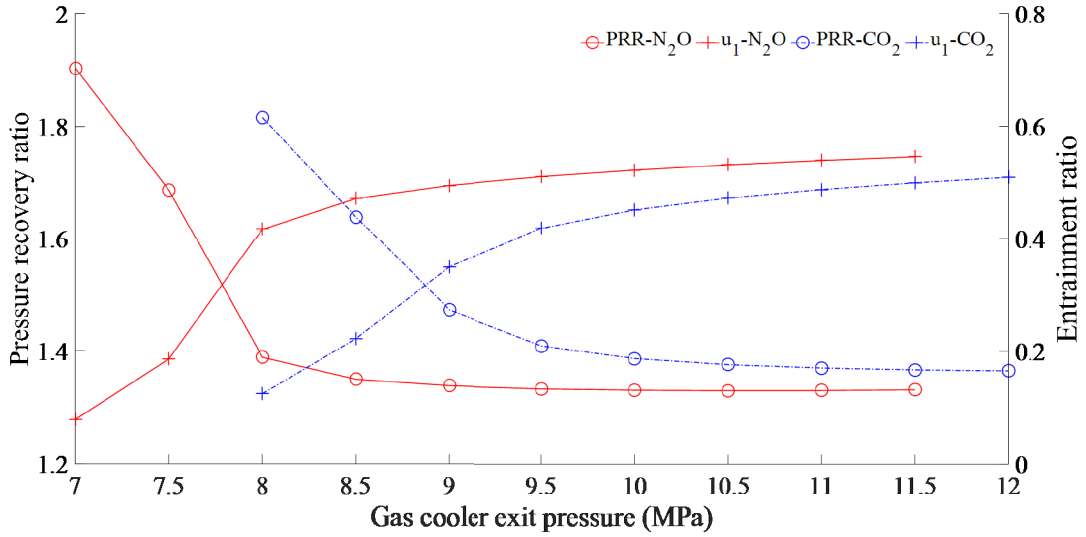

FIGURE 3.46: Effect of gas cooler exit pressure on ejector performance.

3.47) shows the effect of LT evaporator temperature on the system performance at fixed inlet condition of the motive nozzle (P_{gco} = 9 MPa; T_{gco} = 40°C) and MT evaporation temperature (T_{MT} = 0°C). It is observed that COP for both refrigerants shows an increasing trend with the increase in evaporator temperature. It is also observed that COP and second law efficiency of DERC using R744A refrigerant have overall higher COP compared to R744 refrigerant. Further, the second law efficiency of the system shows an overall constant trend. Therefore, it can be concluded that the system second law efficiency is not sensitive to the variation of the LT evaporator temperature.

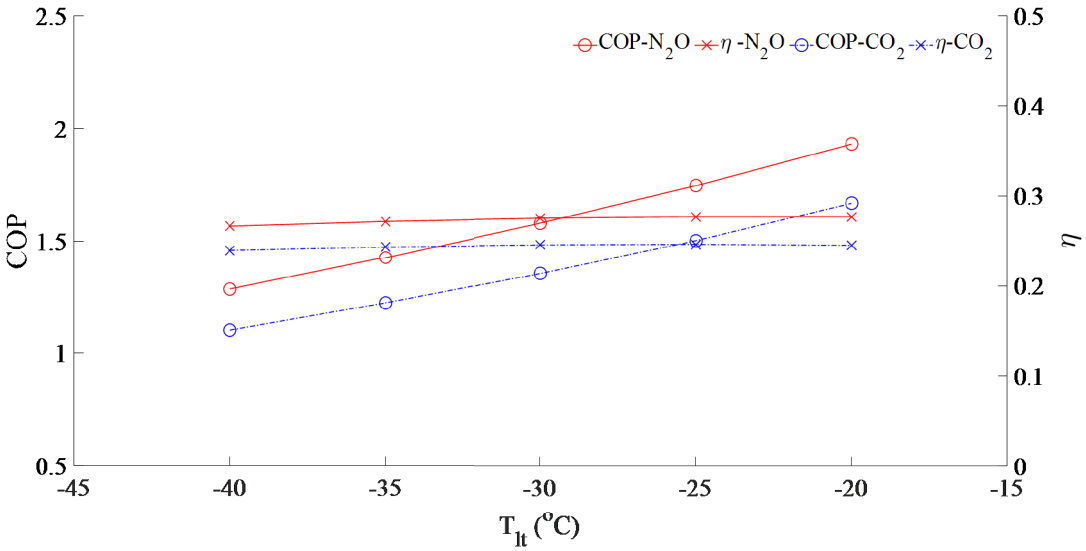

FIGURE 3.47: Effect of lower temperature evaporator on system performance.

3.48) shows the effect of lower temperature evaporator on ejector performance for fixed MT evaporation temperature ($T_{MT} = 0°C$). It is observed that the pressure recovery ratios PRR1, PRR2, and PRR tend to decrease while, entrainment ratios u_1, and u_2 show a slight increment with an increase in LT evaporation temperature. It can be explained as when LT evaporation temperature decreases, the evaporation pressure also decreases which leads to increment in enthalpy difference in the evaporator. Further, refrigerant quality at the ejector-1 outlet would decrease with a decrease in LT evaporation temperature. It tends to increase the mass flow rate in the LT evaporator to meet the fixed refrigeration capacity ratio.

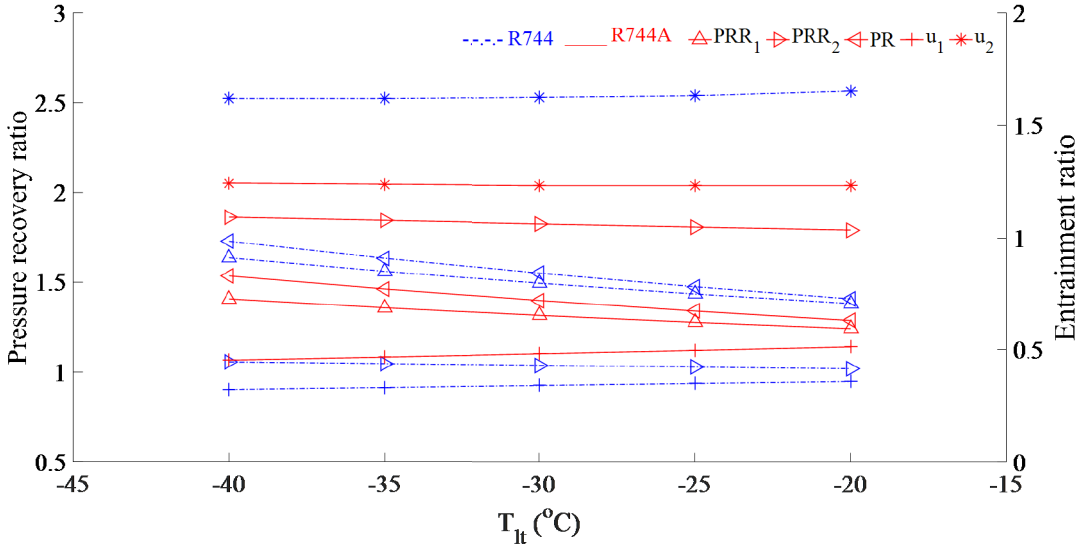

FIGURE 3.48: Effect of lower temperature evaporator on ejector performance.

3.9.3 Comparison based on exergy

3.49)

for maximum COP condition. The exergy output of R744A EETRC is found higher compared to R744 EETRC which implies that the R744A cycle utilizes the available energy more effectively at the specified condition. Further, the most irreversible components identified are the gas cooler, the compressor, and the ejector for both the cycles. Exergy destruction of ejector in R744A EETRC is lesser compared to the R744 cycle which shows that the ejector is quite effective in R744A transcritical refrigeration cycle.

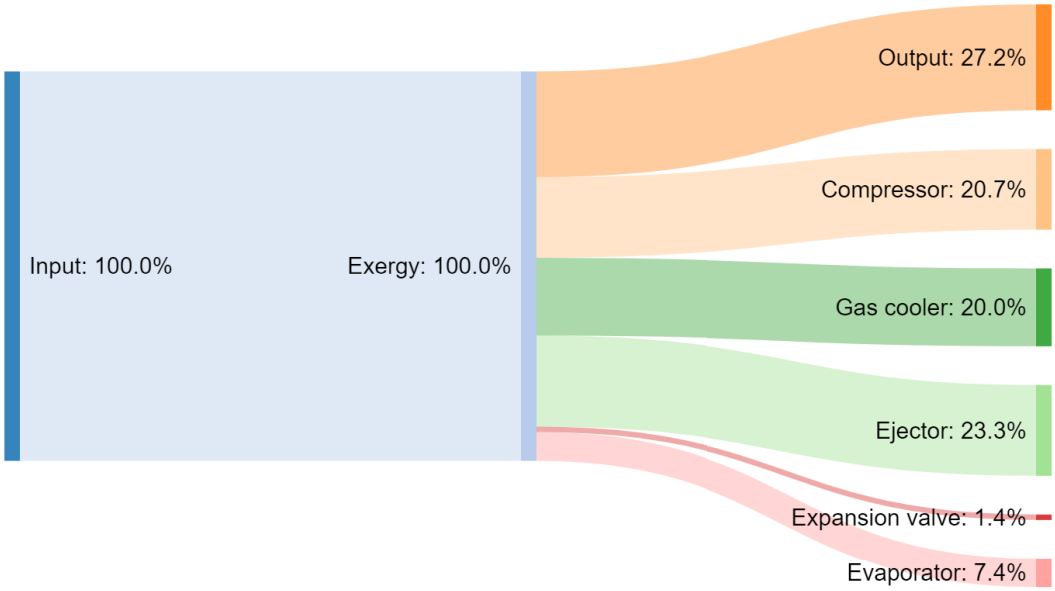

(A) Single Ejector R-744 refrigeration system.

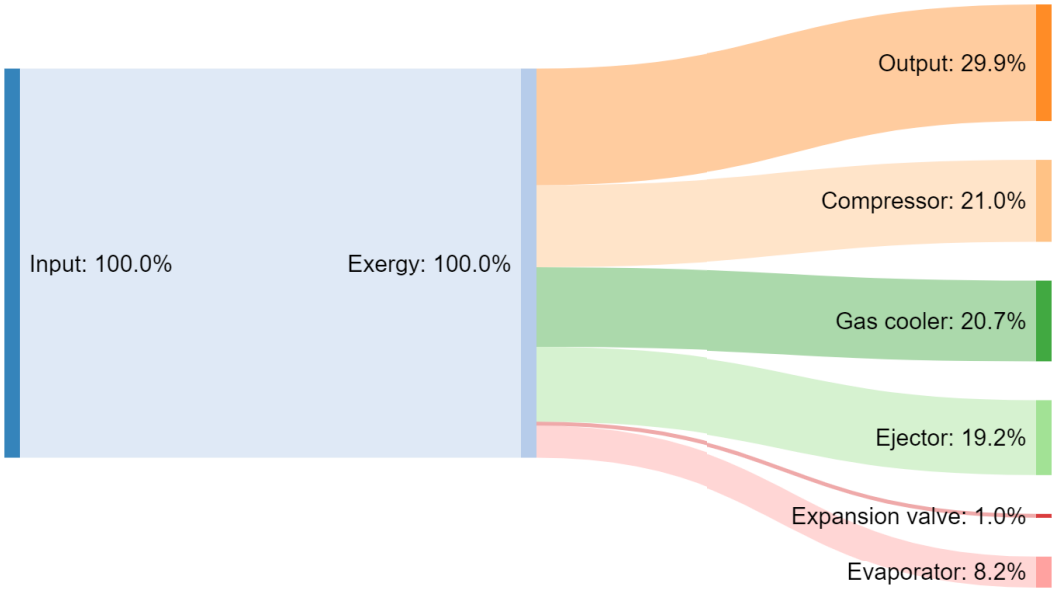

(B) Single Ejector R-744A refrigeration system

FIGURE 3.49: Component wise exergy destruction (Grassman chart)

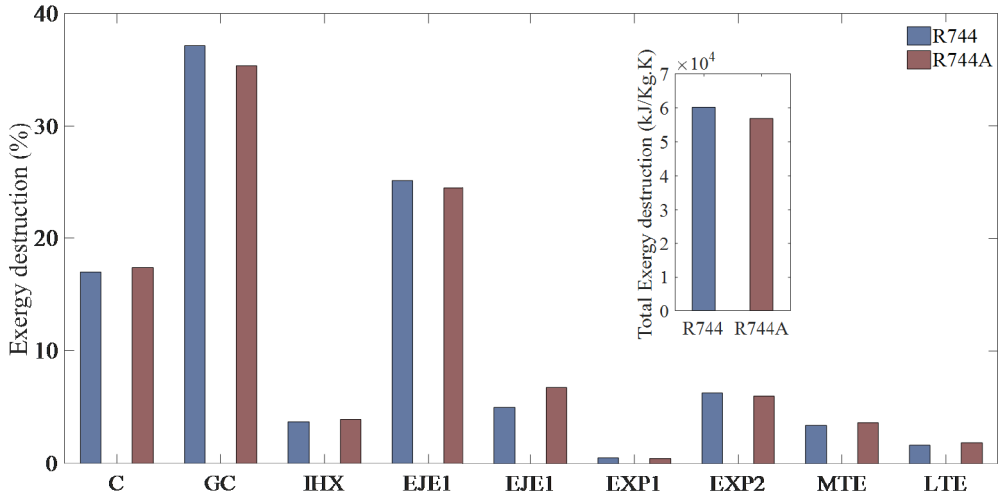

FIGURE 3.50: Percentage contribution of each component to the multi ejector system exergy destruction.

3.50) summarizes the percentage contribution of components to system exergy destruction at fixed operating condition ($T_{gco} = 40°C$; $T_{MT} = 0°C$; $T_{LT} = -25°C$). Gas cooler exit pressure is limited to maximum COP condition (for R-744 $P_{gco} = 10$ MPa; and for R-744A $P_{gco} = 8.5$ MPa). The gas cooler is found to have the highest exergy destruction followed by ejectors and compressors. It is also concluded that exergy destruction is higher for the R744 system compared to the R744A system. The overall exergy efficiency of the R744A system is about 2.51% to 6.56% higher than the R744 system.

3.10 Summary

This chapter presents a systematic investigation of the ejector expansion R-744 refrigeration systems based on the first and second law of thermodynamics for various operating parameters. Initially, models of ejector expansion R-744 transcritical refrigeration system are investigated and compared on the basis of performance parameters such as COP, compressor work, pressure recovery, entrainment ratio, vapor quality, ejector efficiency and exergy. Further, effect of suction nozzle pressure drop is investigated and optimum suction nozzle pressure drop for various P_{gco}, T_{gco} and different ejector nozzle efficiencies are provided. Effect of subcooling on system performance parameters is also investigated. Year-round operational strategy is investigated for thirty different cities which are spread across five climatic zones in India. Environmental impact of the systems is also investigated. Finally, this chapter also includes an investigation of the multi ejector R-744 systems. A comparison is also presented between the performance of R-744 and R-744A systems.